JACS Au
AN OPEN ACCESS JOURNAL OF THE AMERICAN CHEMICAL SOCIETY

pubs.acs.org/jacsau

Article

Zooming into the Inner Helmholtz Plane of Pt(111)−Aqueous Solution Interfaces: Chemisorbed Water and Partially Charged Ions

Jun Huang*

Cite This: https://doi.org/10.1021/jacsau.2c00650

Read Online

ACCESS | Metrics & More | Article Recommendations | Supporting Information

ABSTRACT: The double layer on transition metals, *i.e.*, platinum, features chemical metal−solvent interactions and partially charged chemisorbed ions. Chemically adsorbed solvent molecules and ions are situated closer to the metal surface than electrostatically adsorbed ions. This effect is described tersely by the concept of an inner Helmholtz plane (IHP) in classical double layer models. The IHP concept is extended here in three aspects. First, a refined statistical treatment of solvent (water) molecules considers a continuous spectrum of orientational polarizable states, rather than a few representative states, and non-electrostatic, chemical metal−solvent interactions. Second, chemisorbed ions are partially charged, rather than being electroneutral or having integral charges as in the solution bulk, with the coverage determined by a generalized, energetically distributed adsorption isotherm. The surface dipole moment induced by partially charged, chemisorbed ions is considered. Third, considering different locations and properties of chemisorbed ions and solvent molecules, the IHP is divided into two planes, namely, an AIP (adsorbed ion plane) and ASP (adsorbed solvent plane). The model is used to study how the partially charged AIP and polarizable ASP lead to intriguing double-layer capacitance curves that are different from what the conventional Gouy−Chapman−Stern model describes. The model provides an alternative interpretation for recent capacitance data of Pt(111)−aqueous solution interfaces calculated from cyclic voltammetry. This revisit brings forth questions regarding the existence of a pure double-layer region at realistic Pt(111). The implications, limitations, and possible experimental confirmation of the present model are discussed.

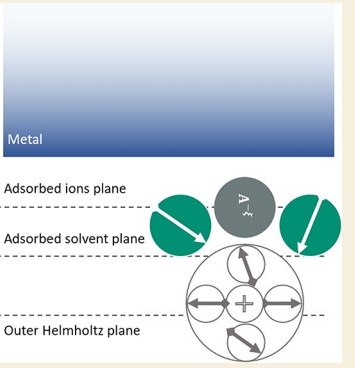

KEYWORDS: *electric double layer, metal−water interactions, specific adsorption, partial charge transfer, water chemisorption, inner Helmholtz plane, pseudo-capacitance, double layer capacitance*

INTRODUCTION

There is a wave of renewed interest in the electric double layer (EDL) structure in electrocatalysis, probably due to two reasons.[1−4] On the one hand, the activity of many electrocatalytic reactions is revealed to be affected markedly by electrolyte cations[5−9] and pH.[10−13] There is growing consensus that demystifying these electrolyte effects requires fundamental knowledge of the EDL,[3,14] as discussed in several review articles.[14−17] On the other hand, a growing body of experimental data on the EDL of single crystals of transition metals, notably platinum, has been reported recently.[4,18−23] These new data, though not fully consistent as detailed below, have already surprised us as they do not agree, even qualitatively, with classical double layer models.

A well-documented classical model is the Gouy−Chapman−Stern (GCS) model, which describes the EDL as a series combination of an inner layer and a diffuse layer.[24] The GCS model has many variants, with detailed treatments of the diffuse layer and the inner layer.[25−27] A hallmark of GCS-like models is the appearance of a minimum in the differential double-layer capacitance (C_{dl}) curve, named the Gouy−Chapman minimum, at a particular electrode potential, named the potential of zero charge (pzc), in dilute electrolyte solutions. Unless otherwise noted, pzc refers to potential of zero free charge. Moving away from the pzc in cathodic and anodic directions, C_{dl} grows and then decreases, resulting in a camel-shaped C_{dl} profile with two peaks and one valley. The two peaks usually signify overcrowding of counterions near the metal surface, which are usually asymmetric due to different sizes of cations and anions. The two peaks move closer and eventually melt into a single peak as the electrolyte solution gets more and more concentrated.[28,29]

The aptness of the GCS model has been corroborated on mercury-like electrodes, first by Gouy in the 1910s[30] and then by Grahame in the 1940s and 1950s,[31] *e.g.*, see Parsons's review.[32] In the presence of specific adsorption of anions, Grahame discriminated an inner Helmholtz plane (IHP) and an outer Helmholtz plane (OHP) in the inner layer.[31] More than just a refinement of the Stern model, the Grahame model sowed the

Received: December 1, 2022
Revised: January 13, 2023
Accepted: January 13, 2023

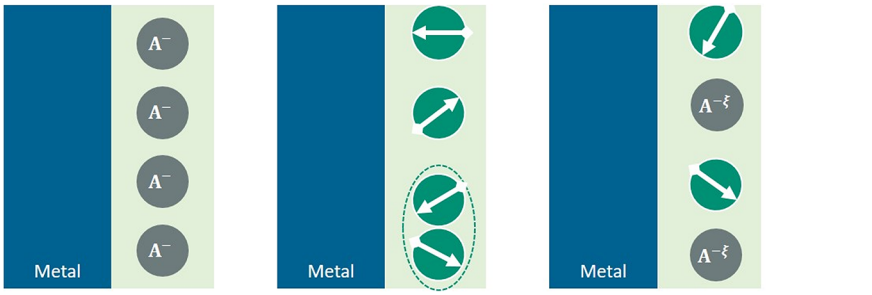

Figure 1. Models of the inner Helmholtz plane (IHP). (a) Grahame−Parsons model views the IHP as an ionic layer where specifically adsorbed ions are rigidly aligned.[31,55,56] (b) Many models are focused on the field-dependent behaviors of solvent molecules, most often water molecules, at the IHP.[34,36,63] (c) Recent models consider the coexistence of solvent molecules and partially charged chemisorbed ions ($A^{-\xi}$) at the IHP.[72,73]

seeds of subsequent developments in the EDL theory, including the consideration of field-dependent orientation of water molecules,[33−36] discreteness of adsorbed ions,[37−40] and quantum effects of metal electrons,[41−44] as discussed in a recent tutorial.[27] Valette and Hamelin and coworkers have demonstrated that the GCS model is valid also for silver single crystals in nonspecifically adsorbing electrolytes.[45−48]

The idyll reaches an end for platinum. The Gouy−Chapman minimum is absent in the study of Pajkossy and Kolb where C_{dl} of Pt(111) in a $KClO_4$ and $HClO_4$ mixture electrolyte with a concentration down to 1 mM was measured.[18,20,49] Instead, their data show a C_{dl} peak near the pzc in the anodic direction. Contrarily, Xue et al. observed Gouy−Chapman minima for Pt(111) in 0.05 M $MeClO_4$ electrolytes (Me = Li, Na, K, Rb, Cs), however, at potentials ∼0.2 V below the pzc.[23] More recently, Ojha et al. observed the Gouy−Chapman minimum for Pt(111) in 0.1 mM $HClO_4$.[21,22] In addition, they found that the Gouy−Chapman minimum turns into a maximum near the pzc when increasing the electrolyte solution above 1 mM, qualitatively consistent with previous observations of Pajkossy and Kolb.[18,20,49]

One should be aware of the discrepancy in the magnitude of C_{dl} of Pt(111) at the pzc, denoted $C_{dl,\,pzc}$, in different studies. $C_{dl,\,pzc}$ is around 20 μF cm^{-2} in the study of Pajkossy and Kolb using an electrolyte concentration of 0.1 M,[18,20,49] in the range of 10−30 μF cm^{-2} for 0.05 M NaOH and 0.10 M $HClO_4$ in the study of Schouten et al.,[50] around 30 μF cm^{-2} in the study of Xue et al. with an electrolyte concentration of 0.05 M,[23] and around 100 μF cm^{-2} in the study of Ojha et al. with an electrolyte concentration of 0.005 M.[21,22] Note that $C_{dl,\,pzc}$ shall decrease with the electrolyte concentration, according to the GCS model. Surprisingly enough, recent values of $C_{dl,\,pzc}$ in more dilute electrolyte solutions are even several times higher than previous values in more concentrated electrolyte solutions. Understanding the origin of the anomalously large $C_{dl,\,pzc}$ is an open question on which several viewpoints already exist, which I am about to discuss, and that motivates this study.

To rationalize the large $C_{dl,\,pzc}$, Doblhoff-Dier and Koper introduced weak (around several hundred meV), attractive ion−surface interaction, of which possible origins are also discussed.[51] This effectively increases the ion concentration in the double layer, shortens the Debye length, and magnifies the magnitude of $C_{dl,\,pzc}$. Recently, Schmickler rationalized the higher $C_{dl,\,pzc}$ as a consequence of weak specific adsorption of anions.[52] The introduction of anion adsorption can increase the overall capacitance, and decrease the Parsons−Zobel slope. However, this model cannot explain that the Parsons−Zobel slopes are not sensitive to the identity of electrolyte anions.[22] More recently, Ojha, Doblhoff-Dier, and Koper modified their previous model by further adopting a two-state submodel for the first-layer water molecules,[22] which was developed earlier by Le et al.[53]

This marked and surprising discrepancy in $C_{dl,\,pzc}$ might be ascribed to different methods used to determine C_{dl}. Pajkossy and Kolb extracted C_{dl} from electrochemical impedance spectroscopy (EIS) data using the Frumkin−Melik−Gaikazyan (FMG) model.[18,20,49] Xue et al. extracted C_{dl} from EIS data using an electric circuit model involving empirical constant phase elements.[23] Ojha et al. calculated C_{dl} from cyclic voltammogram (CV) data.[21,22] EIS is, in principle, more accurate than CV in determining C_{dl}, because EIS can separate C_{dl} from possible pseudo-capacitances of chemisorption. In the presence of chemisorption, the FMG model expresses the total capacitance as $C_{total}(\omega) = C_{dl} + \frac{C_{ad}}{1 + \sqrt{j\omega}\,\sigma_{ad}C_{ad} + j\omega C_{ad}R_{ad}}$, where C_{dl} is the pure double layer capacitance, R_{ad} is the adsorption resistance, C_{ad} is the adsorption capacitance, σ_{ad} is the coefficient of Warburg diffusional impedance, and ω is the angular frequency. Only when $\omega \gg \omega_c = (C_{ad}R_{ad})^{-1}$ can one approximate $C_{total}(\omega)$ as C_{dl}. At low frequencies, one will find $C_{total}(\omega) \approx C_{dl} + C_{ad}$. Earlier studies have shown that ω_c is around 1 MHz for hydrogen adsorption at Pt(111) in 0.5 M perchloric acid[54] and above 10 kHz for hydroxyl adsorption at Pt(111) in 0.1 M perchloric acid.[50] A CV measurement with a scanning rate of 50 mV s^{-1} over a potential range of 0.05 V consumes 1 s and, hence, has a characteristic frequency of 1 Hz, which is far lower than the typical ω_c of Pt(111) electrode processes. Ojha et al. reported the capacitance calculated from impedance at a single frequency of 18 Hz, which is also much below ω_c.[22]

The fact that the CV-derived capacitance is much higher than the EIS-derived capacitance could be attributed to pseudo-capacitances of chemisorption. Based on this assumption, a theory for the large CV-derived capacitance of Pt(111) in the double layer region is developed in this paper. I am about to show that chemisorption at a small percentage of platinum sites can explain the observed large capacitance.

The remainder of this paper is organized as follows. First, I present a short review of the developments on the IHP model after the pioneering works of Grahame and Parsons.[55,56] Most of these important works that adequately reflect the depth, core, and beauty of electrochemical research are less known and only sparsely cited nowadays. This literature review also sets the baseline for the present model, which is not entirely new, but

https://doi.org/10.1021/jacsau.2c00650
JACS Au XXXX, XXX, XXX−XXX

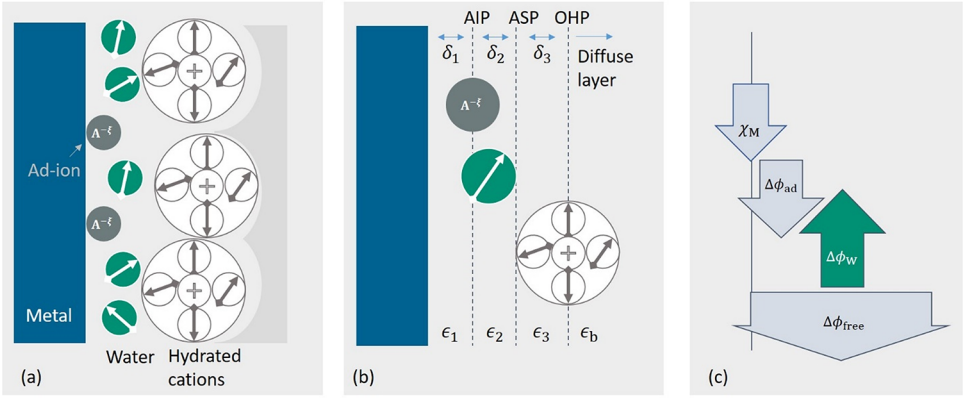

Figure 2. (a) Schematic illustration of the electrocatalytic double layer with partially charged, chemisorbed ions, adsorbed solvent (water in this case) molecules, and nonspecifically adsorbed ions. (b) Continuum EDL model consists of an AIP denoting the central plane of chemisorbed ions, an ASP denoting the outer plane of adsorbed water molecules, and an OHP denoting the central plane of nonspecifically adsorbed ions. The regions between the metal and the AIP, the AIP and the ASP, and the ASP and the OHP are described as dielectric continua, parameterized with respective thicknesses δ_i and permittivities ϵ_i, with i = 1,2,3. (c) Overall potential difference between the metal bulk and the solution bulk can be divided into four components: χ_M denoting the potential drop at the metal surface due to electron distribution, $\Delta\phi_{ad}$ the potential change due to partially charged, chemisorbed ions, $\Delta\phi_w$ the potential change due to orientational polarization of adsorbed water molecules, and $\Delta\phi_{free}$ the potential change due to excess ionic charge stored in the diffuse layer, namely, free surface charge.

extends previous models in some aspects. Second, a detailed derivation of the model, including a water layer submodel and a chemisorption submodel, is presented. Third, the model is demystified for two cases. In the first case without chemisorbed ions, emphasis is put on understanding how metal−water interactions change the pzc and the double layer capacitance. For the second case with chemisorbed ions, emphasis is put on the consequence of chemisorption-induced surface dipole moment. The model is then used to interpret recent experimental data of Ojha et al.[21,22] in the double layer region. This revisit questions current fundamental understanding of the EDL at Pt(111). Lastly, discussion on assumptions, implications, and possible extensions of the model is presented before the conclusion section.

MODELS OF THE IHP: GRAHAME−PARSONS MODEL AND BEYOND

Above analysis has turned the spotlight on the IHP in understanding the EDL at transition metals. Figure 1 summarizes three groups of IHP models. The Grahame−Parsons model views the IHP as an ionic layer with specifically adsorbed ions rigidly lining up.[31,55,56] The potential drop from the metal surface to the IHP is composed of two parts. The first part is due to the metal surface charge, and the second part is the net charge of specifically adsorbed ions at the IHP. There is no electron transfer during specific ionic adsorption; hence, the specifically adsorbed ions retain the charge they have in the bulk solution. In the literature, *e.g.*, ref 57, there is another Grahame−Parsons model, which describes the thermodynamics of specific ion adsorption, and determines the coverage of adsorbed ion as a function of the electrode potential. The Grahame−Parsons model of ion adsorption was later improved by the Alexeyev−Popov−Kolotyrkin model[58] and the Vorotyntsev model.[59]

Another group of IHP models focuses on solvent molecules at the IHP in the absence of specifically adsorbed ions, (Figure 1b); see an earlier review by Guidelli.[60] The two-state model assumes that water molecules take either the hydrogen-up or hydrogen-down configuration, depending on the local electric field.[34] The three-state model further considers formation of water dimers and interconversion between water dimers and monomers.[36] Both models are founded purely on electrostatic considerations; thus, the average dipole moment of the water layer is zero when the metal surface has a zero net charge. In addition to electrostatic interactions, chemical interactions between water molecules and the metal surface were speculated in the 1970s.[61] Damaskin and Frumkin considered both electrostatic and chemical metal−water interactions at the IHP.[62] Electrostatic interactions are treated using the approach of Bockris, Devanathan, and Miller (BDM),[63] which does not consider properly the configurational entropy. The fraction of chemisorbed water molecules was expressed phenomenologically as an exponential function of the electrode charge. Recently, we have seen a surge of atomistic simulations of water molecules near metal surfaces.[53,64−68] These first-principles calculation results provide unbiased, accurate atomistic details, guiding the development of phenomenological models, as demonstrated in the work by Le et al.[53]

In most cases, the IHP is neither an ionic layer nor a solvent layer. Instead, it is a mixture of solvent molecules and chemisorbates. Chemisorbates, usually partially charged due to partial charge transfer, contribute an additional potential drop in the inner layer.[69] Therefore, a refined model of the IHP should be a binary IHP model that considers co-existing solvent molecules and partially charged ions. Carnie and Chan developed a so-called civilized model of EDLs, which considers ions as hard spheres with embedded point charge (integral charges, rather than partial charges), and solvent molecules as hard spheres with embedded dipole moment in the 1980s.[70] The Carnie−Chan model was used to calculate the dipole moment of specifically adsorbed ions at the IHP.[71] More recently, the binary IHP model was further extended to consider potential-varying coverage of partially charged chemisorbates.[72,73] More than just a further complication of a model, it brings forth nontrivial implications of chemisorption-induced surface dipole moment (μ_{chem}). It was revealed that μ_{chem} of adsorbed hydroxyl leads to a nonmonotonic surface charging behavior of Pt(111)−aqueous solution interfaces. Specifically, the free charge, not the total charge nor the metal charge,[74] exhibits a negative−positive−negative transition with increasing electrode potential. This implies the occurrence of negative C_{dl} and more than one

https://doi.org/10.1021/jacsau.2c00650
JACS Au XXXX, XXX, XXX−XXX

potential of zero free charge. Nonmonotonic surface charging behaviors of a polycrystalline Pt electrode were measured using the radioactive tracers method by Frumkin and co-workers[75,76] and later in several experiments of laser-induced potential transients.[77−79] The nonmonotonic surface charging behaviors were modeled earlier by assuming that the pzc grows linearly with the coverage of adsorbed oxygen and later by a phenomenological treatment in which the potential drop in the IHP is interpolated between two limiting states.[76] The model developed in refs 72 and 73 and later modified in ref 80 provides a consistent treatment of chemisorption and surface charging behaviors as a function of electrode potential. It was also shown in ref 72 that orientational polarization of interfacial water molecules, described using the two state model, leads to a negative capacitive component to C_{dl}, an effect that was later elucidated in greater detail by Le et al.[53]

The IHP model that I am about to present in this paper improves over the previous one in refs 72 and 73 in three aspects. First, the present model abandons the BDM-type two-state water model and adopts a statistical treatment of water polarization with a continuum spectrum of orientational states, following the approach developed earlier in refs 81 and 82. The configurational entropy of water molecules at the IHP is considered. In addition to electrostatic interactions, chemical interactions with the metal are considered, as inspired by ab initio molecular dynamics (AIMD) results,[53,66,67] but in a different manner compared to the Damaskin−Frumkin model. Second, chemisorption at the IHP is now energetically distributed in such a way that the equilibrium potential follows a distribution instead of taking a single value as usual. This allows treatment of chemisorption at different types of active sites, chemisorption of different species, and lateral interactions between chemisorbates in a unifying manner. Third, as suggested by recent detailed atomistic simulations, *e.g.*, ref 83, the IHP is further divided into an adsorbed ion plane (AIP) and an adsorbed solvent plane (ASP). This refinement is necessary because the AIP and ASP have very different properties, which I am about to show in model parameterization.

THEORETICAL METHODS

Physical Picture of the Double Layer

A schematic illustration of an electrocatalytic double layer is presented in Figure 2a, and a continuum model is depicted in Figure 2b. The metal electrode is assumed to be planarly uniform. Surface roughness is not considered here. The first-layer water molecules are usually highly polarized due to the high interfacial electric field and chemical interactions with the metal; see a recent review by Groß and Sakong.[68] The ASP denotes the outer plane of adsorbed solvent molecules. Adsorbed ions, if any, are usually located closer to the metal surface than adsorbed solvent molecules, according to atomistic simulations, *e.g.*, by Braunwarth et al.[83] The central plane of adsorbed ions is denoted AIP. Different characteristic planes are used for depicting the ASP and AIP due to difference between ionic charge and dipolar charge. Nonspecifically adsorbed ions with their solvation shell reside in the diffuse layer stretching from the OHP toward the solution bulk. The regions between the metal and the AIP, the AIP and the ASP, and the ASP and the OHP are described as dielectric continua, parameterized with thicknesses δ_i and permittivities ϵ_i, with i = 1,2,3.

Potential Differences in Different Components

As EDL is a grand canonical system with electrode potential being one of the independent variables, the overarching task of any EDL model is to calculate the electric potential distribution from the metal to the electrolyte solution. Figure 2c depicts components of the overall potential difference between metal bulk (ϕ_M) and solution bulk (ϕ_S). At the metal surface exists a large potential drop due to the metal electron tail, denoted χ_M, which is readily obtained from electronic structure calculations, *e.g.*, in ref 84. There are, at least, three other potential differences, including one due to partially charged, chemisorbed ions, one due to adsorbed solvent (water in this work) molecules, and one due to the free surface charge density, σ_{free}, defined as negative of the net ionic charge in the diffuse layer.[80]

The above decomposition scheme, following ref 85, is expressed as

$$\phi_M - \phi_S = \chi_M + \Delta\phi_{free} + \Delta\phi_{ad} + \Delta\phi_w \tag{1}$$

Within a continuum picture, $\Delta\phi_{free}$ is written as

$$\Delta\phi_{free} = \mathrm{sign}(\sigma_{free})\frac{2RT}{F}\mathrm{arsinh}\left(\sqrt{\frac{1}{2\gamma}\left(\exp\left(\frac{\gamma}{2}\left(\frac{F\lambda_D\sigma_{free}}{2RT\epsilon_b}\right)^2\right)-1\right)}\right) + \sigma_{free}\sum_{i=1,2,3}\frac{\delta_i}{\epsilon_i} \tag{2}$$

where the first term denotes the potential change over the diffuse layer, which is derived from the Bikerman model considering finite ion size,[28,73] $\lambda_D = \sqrt{\epsilon_b RT/2c_b F^2}$ is the Debye length, ϵ_b is the dielectric permittivity of the bulk solution, c_b is the bulk ion concentration, R is the gas constant, F is the Faraday constant, T is the temperature, and $\gamma = 2c_b d_h^3$ with d_h being the diameter of hydrated ions. Size asymmetry of cations and anions is not considered here, for the sake of an analytical expression of $\Delta\phi_{free}$ as a function of σ_{free}, and effects of size asymmetry on the C_{dl} are known already.[86−89]

The other two components $\Delta\phi_{ad}$ and $\Delta\phi_w$ are determined from two submodels as introduced below.

Distributed Chemisorption Model

The amount of charge carried by partially charged, chemisorbed ions at the AIP is calculated as, $-\sum_A N_{ad}\theta_A e_0 \xi_A$, where N_{ad} is the number density of adsorption sites, θ_A and ξ_A are the coverage and net electron of a chemisorbed ion of type A, and e_0 is the elementary charge.[80] The parameter ξ_A is related to the partial charge transfer coefficient, λ_A, via $\xi_A = z_A + \lambda_A$, with z_A being the initial charge of chemisorbed ions. A total charge transfer process corresponds to, $\lambda_A = -z_A$. Note in passing that the net charge ξ_A and the partial charge transfer coefficient λ_A are different from the electrosorption valency that can be measured experimentally.[85]

$\Delta\phi_{ad}$ is then calculated as the potential difference across an equivalent planar capacitor with a charge amount of $\sum_A N_{ad}\theta_A e_0 \xi_A$ on each side

$$\Delta\phi_{ad} = \frac{\delta_1}{\epsilon_1}\sum_A N_{ad}\theta_A e_0 \xi_A \tag{3}$$

A positive-valued ξ_A means negatively charged chemisorbed ions, which introduces a positive $\Delta\phi_{ad}$. A chemisorption submodel is required to determine θ_A as a function of the electrode potential.

For chemisorption of hydrogen, $H^+ + e + * \leftrightarrow H_{ad}$, the Frumkin isotherm gives[90,91]

$$\ln\left(\frac{\theta_H}{\theta_{H,max}-\theta_H}\right) + \gamma_H\theta_H = -\beta(E_{RHE} - E_H^0) \tag{4}$$

where θ_H is the coverage of H_{ad}, $\theta_{H,max}$ is the maximum coverage, γ_H is the lateral interaction coefficient, $\beta = F/RT$, and E_H^0 is the equilibrium potential on the standard hydrogen electrode (SHE) scale. Recently, Hormann et al. has illustrated how to obtain E_H^0 and γ_H from density functional theory (DFT) calculations.[92] The existence of lateral interactions stands in the way of obtaining an analytical solution for θ_H.

The Frumkin isotherm can be transformed into a series of Langmuir-type isotherms with a distributed E_H^0,

$$\left\{\ln\left(\frac{\theta_H}{\theta_{H,max}-\theta_H}\right) = -\beta(E_{RHE} - E), f_H(E)\right\} \tag{5}$$

https://doi.org/10.1021/jacsau.2c00650
JACS Au XXXX, XXX, XXX−XXX

where $f_H(E)$ denotes the probability of an equilibrium potential at E.

The distribution in equilibrium potential can be ascribed to the existence of structural defects, lateral interactions that change the electrochemical potential for later adsorbates, and a potential-dependent distribution in the electrochemical potential of reactants, among others. I will go back to this in the discussion section.

As any distribution can be expanded as a series of normal distributions, E_H^0 is assumed to take the following general form,

$$f_H(E) = \sum_k p_k g_k(E; \mu_k, \sigma_k) \tag{6}$$

where $g_k(E; \mu_k, \sigma_k)$ are normal distributions of weight p_k, expectations μ_k, and variances σ_k

$$g_k(E; \mu_k, \sigma_k) = \frac{1}{\sigma_k\sqrt{2\pi}}\exp\left(-\frac{1}{2}\left(\frac{E-\mu_k}{\sigma_k}\right)^2\right) \tag{7}$$

and $\sum_k p_k = 1$ for the weight values.

Now, θ_H is expressed analytically as

$$\theta_H = \int dE f_H(E)\theta_{H,max}\frac{\exp(-\beta(E_{RHE}-E))}{1+\exp(-\beta(E_{RHE}-E))} \tag{8}$$

Similarly, the coverage of adsorbed OH is written as

$$\theta_{OH} = \int dE f_{OH}(E)\theta_{OH,max}\frac{\exp(\beta(E_{RHE}-E))}{1+\exp(\beta(E_{RHE}-E))} \tag{9}$$

where $f_{OH}(E)$ is the distribution function of the equilibrium potential of OH adsorption, which has the same form as eq 6.

The pseudo-capacitance of chemisorption of H_{ad} and OH_{ad} is calculated as

$$C_{A_{ad}} = \mp N_{ad} e_0 \frac{d\theta_A}{dE_{RHE}} \tag{10}$$

with A = H (−) or OH (+).

Cautious readers may think a term $(1 \pm \xi_A)$ (+ for H_{ad} and − for OH_{ad}) should be added in eq 10 to account for the partial charge transfer. This is unnecessary because no matter how the electron is partitioned between the metal and the adsorbate, one electron is taken out from or moved into the electrode, if we separate the total surface charge into σ_{free} and the charge involved in specific adsorption of ions. I will explain this point later when discussing the relationship between the total capacitance, $C_{A_{ad}}$, and C_{dl} in eq 24.

The Frumkin isotherm can be regarded as a Langmuir isotherm with the equilibrium potential linearly varying with the adsorbate coverage, with the linear coefficient being the lateral interaction coefficient. In this sense, the distribution function expressed in eq 6 is just a generalization of the Frumkin isotherm. In fact, the linear coverage dependence of the equilibrium potential has no fundamental reason but is just a first approximation. Nonlinear effects have been observed in many cases such as the chemisorption of OH at Pt(111) in the study of Climent et al.[91] The exact form of $f_A(E)$ corresponding to the Frumkin isotherm is unknown currently. However, I will extract $f_H(E)$ and $f_{OH}(E)$ from experimental CVs that are usually fitted using Frumkin isotherms.

Water Model with a Continuous Spectrum of Orientational States

The last term in eq 1 is the potential difference due to the average dipole moment of the first-layer water molecules,

$$\Delta\phi_w = -\frac{N_{ad}\theta_w}{\epsilon_2}\mu_w\langle\cos\alpha_w\rangle \tag{11}$$

where θ_w is the coverage of water molecules, μ_w is the dipole moment of a water molecule, and $\langle\cos\alpha_w\rangle$ is the statistical average of $\cos\alpha_w$ with α_w being the angle between water dipoles and the local electric field, as depicted in Figure 3. Herein, a positive electric field points toward the bulk solution, and the direction of a dipole points from its negative end to its positive end.

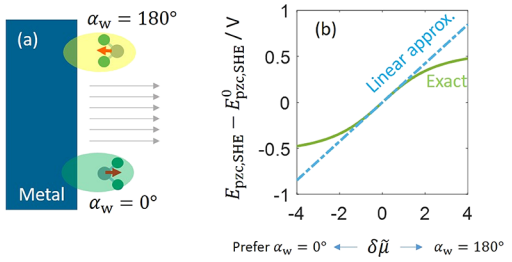

Figure 3. (a) α_w is the angle between water dipoles and the local electric field. A positive electric field points toward the bulk solution, and the direction of a dipole points from its negative end to its positive end. Chemical metal−water interactions result in an energy difference between water of $\alpha_w = 0°$ and that of $\alpha_w = 180°$, denoted $\delta\mu$. (b) Shift in the potential of zero charge as a function of $\delta\tilde{\mu}$ (the solid line: exact results, the dotted line: linear approximation). The calculation uses the following set of model parameters: $N_{ad} = 0.15$ Å^{-2}, $\theta_w = 0.5$, $\epsilon_2 = 3.25\epsilon_0$, $\mu_w = 0.73$ D, as discussed in the model parameterization section. Matlab script of this figure is provided in the Supporting Information of this paper.

In this model, α_w could take any value between 0 and 180°, instead of two values in the Watts−Tobin model and the BDM model that were widely adopted in recent work.[53,72] In this sense, the present treatment could be named an infinite-state water model.

Considering a canonical ensemble consisting of N_w water molecules at the IHP, at the mean-field level, the Hamiltonian of this canonical ensemble is written as

$$\mathcal{H}_w = \sum_i (\mu_w E_{loc} + \delta\mu)\cos(\alpha_i) \tag{12}$$

where α_i is the angle between the ith water and the local electric field $E_{loc} = -\frac{\sigma_{free}}{\epsilon_2}$ and $\delta\mu$ is the chemical interaction energy difference between the case of $\alpha_w = 0°$ and the case of $\alpha_w = 180°$; see the illustration in Figure 3a. The introduction of $\delta\mu$ accounts for chemical interactions between water molecules and the metal surface. Damaskin and Frumkin also considered chemical metal−water interactions.[62] A key difference between this water model and the Damaskin−Frumkin model is that a statistical ensemble approach is adopted here.

The partition function of the water layer is written as[93]

$$\Xi_w = \frac{\int_0^{2\pi}\prod_i d\psi_i \int_0^{\pi}\prod_i d\alpha_i \sin\alpha_i \exp(-\mathcal{H}_w/k_BT)}{\left(\int_0^{2\pi} d\psi_i \int_0^{\pi} d\alpha_i \sin\alpha_i\right)^{N_w}} = \left[\frac{\sinh((\mu_w E_{loc}+\delta\mu)/k_BT)}{(\mu_w E_{loc}+\delta\mu)/k_BT}\right]^{N_w} \tag{13}$$

where ψ_i is the longitude of the solid angle.

The Helmholtz free energy of the water layer is calculated as

$$A_w = -k_BT\ln\Xi_w = -k_BTN_w\ln\left[\frac{\sinh((\mu_w E_{loc}+\delta\mu)/k_BT)}{(\mu_w E_{loc}+\delta\mu)/k_BT}\right] \tag{14}$$

The statistical average of $\cos(\alpha_i)$ is calculated as

https://doi.org/10.1021/jacsau.2c00650
JACS Au XXXX, XXX, XXX−XXX

$$\langle \cos \alpha_w \rangle = \frac{\int_0^{2\pi} \prod_i d\psi_i \int_0^{\pi} \prod_i d\alpha_i \sin \alpha_i \cos \alpha_i \exp\left(-\frac{\mathcal{H}_w}{k_B T}\right)}{\int_0^{2\pi} \prod_i d\psi_i \int_0^{\pi} \prod_i d\alpha_i \sin \alpha_i \exp\left(-\frac{\mathcal{H}_w}{k_B T}\right)}$$
$$= \frac{1}{N_w \mu_w} \frac{\partial A_w}{\partial E_{loc}} = -\coth\left(\frac{(\mu_w E_{loc} + \delta\mu)}{k_B T}\right) + \frac{1}{(\mu_w E_{loc} + \delta\mu)/k_B T} \quad (15)$$

Surface Charging Formula

Combining eqs 1, 2, 3, and 11 leads to a formula from which one can solve for σ_{free} as a function of ϕ_M,

$$\mathrm{sign}(\sigma_{free}) \frac{2RT}{F} \mathrm{arsinh}\left(\sqrt{\frac{1}{2\gamma}\left(\exp\left(\frac{\gamma}{2}\left(\frac{F\lambda_D \sigma_{free}}{2RT\epsilon_b}\right)^2\right) - 1\right)}\right) + \sigma_{free} \sum_{i=1,2,3} \frac{\delta_i}{\epsilon_i} + \frac{\delta_1}{\epsilon_1} \sum_A N_{ad} \theta_A e_0 \xi_A - \frac{N_{ad}\theta_w}{\epsilon_2} \mu_w \langle \cos \alpha_w \rangle + \chi_M = \phi_M - \phi_S \quad (16)$$

At the pzc, $\sigma_{free} = 0$, eq 16 is thus simplified to

$$(\phi_M - \phi_S)_0 = \chi_M + \frac{\delta_1}{\epsilon_1} \sum_A N_{ad} \theta_A e_0 \xi_A - \frac{N_{ad}\theta_w}{\epsilon_2} \mu_w \left(\coth(\delta\tilde{\mu}) - \frac{1}{\delta\tilde{\mu}}\right) \quad (17)$$

where the subscript 0 denotes the pzc condition.

If there is no chemisorbed ions at the pzc, eq 16 is further simplified to

$$(\phi_M - \phi_S)_0 = \chi_M + \frac{N_{ad}\theta_w}{\epsilon_2} \mu_w \left(\coth(\delta\tilde{\mu}) - \frac{1}{\delta\tilde{\mu}}\right) \quad (18)$$

where the dimensionless $\delta\tilde{\mu} = \frac{\delta\mu}{k_B T}$ is used.

The potential difference $\phi_M - \phi_S$ at an electrode−electrolyte interface is not measurable without involving its counterpart at a reference electrode[94] and must be differentiated from the electrode potential E in experiments.

Conversion from ($\phi_M - \phi_S$) to Electrode Potential

In potentiostatic experiments, one can control the potential of the working electrode (WE), namely, the metal in Figure 2a, with respect to a reference electrode (RE). The electrode potential is written as $E = \phi_M - \phi_{RE}$ with ϕ_{RE} being the inner potential of the RE, up to an unimportant constant accounting for different work functions of WE and RE materials. The electrode potential could be rewritten as a difference between two potential differences, $E = (\phi_M - \phi_S) - (\phi_{RE} - \phi_S)$. Here, it is assumed that the RE is put in the same electrolyte with the working electrode, and $\phi_{RE} - \phi_S$ is the potential difference between the RE and the electrolyte solution. The reversible hydrogen electrode (RHE) belongs to this case. If the RHE is used as the RE, $(\phi_M - \phi_S)$ becomes

$$(\phi_M - \phi_S) = E_{RHE} + (\phi_{RE} - \phi_S)_{RHE} \quad (19)$$

where the subscript 'RHE' specifies the reference electrode. This equation can be related to the constant inner-potential DFT proposed recently by Melander et al.[95]

According to the Nernst equation, the potential difference of the RHE and that of the standard hydrogen electrode (SHE) are correlated as

$$(\phi_{RE} - \phi_S)_{RHE} = (\phi_{RE} - \phi_S)_{SHE} - (\ln 10)\frac{RT}{F}\mathrm{pH} \quad (20)$$

where $(\phi_{RE} - \phi_S)_{SHE}$ is the value at the SHE.

Combined, eqs 19 and 20 lead to

$$(\phi_M - \phi_S) = E_{SHE} + (\phi_{RE} - \phi_S)_{SHE} \quad (21)$$

given that $E_{SHE} = E_{RHE} - (\ln 10)\frac{RT}{F}\mathrm{pH}$.

Substituting eq 21 into eq 16 gives

$$\mathrm{sign}(\sigma_{free}) \frac{2RT}{F} \mathrm{arsinh}\left(\sqrt{\frac{1}{2\gamma}\left(\exp\left(\frac{\gamma}{2}\left(\frac{F\lambda_D \sigma_{free}}{RT\epsilon_b}\right)^2\right) - 1\right)}\right) + \sigma_{free} \sum_{i=1,2,3} \frac{\delta_i}{\epsilon_i} + \frac{\delta_1}{\epsilon_1} \sum_A N_{ad} \theta_A e_0 \xi_A - \frac{N_{ad}\theta_w}{\epsilon_2} \mu_w \langle \cos \alpha_w \rangle = E_{SHE} + (\phi_{RE} - \phi_S)_{SHE} - \chi_M \quad (22)$$

where $(\phi_{RE} - \phi_S)_{SHE} - \chi_M$ is, in general, a function of E_{SHE}.

Double-Layer and Total Capacitance

In the presence of chemisorption, it is important to distinguish two types of differential capacitance. The differential double-layer capacitance, corresponding to the free surface charge, is defined as

$$C_{dl} = \frac{\partial \sigma_{free}}{\partial E} \quad (23)$$

The total surface charge σ_{total}, of which the change is measurable by counting electrons flowing through the external circuit, is the sum of σ_{free}, corresponding to the excess ionic charge stored in the diffuse layer, and the charge involved by specific adsorption of ions, namely,[74]

$$\sigma_{total} = \sigma_{free} + \sum_A \mp N_{ad} e_0 \theta_A$$

with A = H (−) or OH (+). The differential total capacitance, corresponding to σ_{total}, is thus the sum of C_{dl} and pseudo-capacitances given in eq 10,

$$C_{total} = C_{dl} + \sum_A C_{A_{ad}} \quad (24)$$

It is important to understand that specific adsorption of ions not only contributes to $C_{A_{ad}}$ but also influences C_{dl} via the resultant surface dipole moments.

Model Parameterization

The process of parameterizing a continuum EDL model is more or less a process connecting it to atomistic simulations using Kohn−Sham DFT, reactive force field molecular dynamics (MD), etc. The model contains four groups of parameters. The first group concerns the multilayer structure and dielectric properties of the EDL. The second and third group describe adsorbed water molecules and chemisorbed ions, respectively. The last group defines material properties of the metal and the electrolyte solution.

The first group of parameters includes ϵ_i and δ_i. Recent years have witnessed detailed DFT and MD studies of Pt(111) electrodes with chemisorbed H and OH. Le et al. showed that the density of H_{ad} peaks at ∼1 Å above the metal surface.[67] Braunwarth et al. gave a bond length of 1.05 Å for adsorbed O on Pt(111).[83] Therefore, I use $\delta_1 = 1\mathring{A}$ for the AIP. In the presence of an electron tail in the space between the metal and the AIP, ϵ_1 should be higher than the vacuum permittivity ϵ_0; otherwise, C_{dl} is bounded by $C_{AIP} = 8.85\ \mu F\ cm^{-2}$. Herein, I assume $\epsilon_1 = 10\epsilon_0$ to account for the effects of electrons spilled from Pt(111). These studies also indicated that the adsorbed, first-layer water molecules are around 2.1 $\mathring{A}$ above the metal surface. Therefore, δ_2, the thickness of the gap between the AIP and ASP, is approximated as $\delta_2 = 1.1\ \mathring{A}$. Since orientational (inertial, slow, low-frequency) polarization of water dipoles is explicitly considered in $\Delta\phi_w$, ϵ_2 is the electronic (noninertial, fast, high-frequency) permittivity, which is known to be $\epsilon_2 = 3.25\ \epsilon_0$ at room temperature.[96] Le et al.[67] used $\epsilon_2 = 4\epsilon_0$. An earlier estimate by Bockris et al. reads $\epsilon_2 = 6\epsilon_0$.[63] For the region between the ASP and

https://doi.org/10.1021/jacsau.2c00650
JACS Au XXXX, XXX, XXX−XXX

OHP, I used $\delta_3 = 3.5$ Å, a typical radius of hydrated ions, and $\epsilon_3 = 78.5\ \epsilon_0$, the permittivity of bulk solution.

As for adsorbed water molecules, Le et al. determined a coverage of ~0.5.[53] Hence, I use $\theta_w = 0.5$. Schnur and Groß calculated the adsorption energy of the H-down and H-up water at several solids using an ice-like water bilayer model.[97] The H-down and H-up configurations correspond to $\alpha_w = 180°$ and $\alpha_w = 0°$, respectively. Their data show that $\delta\tilde{\mu} \approx 0$ at Ru(0001) and $\delta\tilde{\mu} \approx 1$ at Au(111), Ag(111), and Pt(111). It is understood that $\delta\tilde{\mu}$ has the unit of k_BT. In more recent AIMD simulations, a more detailed picture of interfacial water molecules has emerged.[53,66,98] At the Pt(111)−water interface, a fraction of water molecules are bound strongly through their oxygen atom with the metal so that the hydrogen atoms of the water molecule are above the oxygen atom. This is called the O-down configuration, corresponding to $\alpha_w = 0°$ in this model. A bit further away from the metal surface resides another type of water molecules, which can be further divided into the H-down ($\alpha_w = 180°$) and H-up ($\alpha_w = 0°$) configurations. These recent AIMD results suggest $\delta\tilde{\mu} < 0$ for the present model. The intrinsic dipole moment of a water molecule is 1.85 D. However, in order to reproduce the permittivity of bulk water using the dipolar Poisson−Boltzmann theory, Abrashkin et al. used an effective value of 4.86 D.[99] Herein, I determine μ_w from the interfacial potential change due to water orientation, which was determined to be −0.2 V for a clean, uncharged Pt(111) surface by Le et al.[65] From eq 22, the present model determines the orientation-induced potential change as $\frac{N_{ad}}{\epsilon_2}\theta_w\mu_w\left(\coth(\delta\tilde{\mu}) - \frac{1}{\delta\tilde{\mu}}\right)$. Assuming $\delta\tilde{\mu} = -1$, I thus determine $\mu_w = \frac{-0.2\epsilon_2}{N_{ad}\theta_w(\coth(-1)+1)} = 0.73$ D. If $\delta\tilde{\mu} = -2$, $\mu_w = 0.43$ D. The lower bound of μ_w is 0.23 D. A lower effective value of μ_w accounts for the unevenness of the first-layer water molecules as well as offset effects by second-layer water molecules.

Malek and Eikerling calculated the work function change due to chemisorbed oxygen at Pt(111), from which they estimated the partial charge residing on each adsorbed oxygen.[100] Using a vacuum permittivity, they determined that each adsorbed oxygen on Pt(111) carries a partial charge of ~0.012e. Since $\epsilon_1 = 10\epsilon_0$ is used here, I should use $\xi_{OH} = 0.12$ to reproduce the same magnitude of work function change induced by chemisorbed ions. Chemisorbed H is assumed to be electroneutral, namely, $\xi_H = 0$. The present model does not need a single-valued equilibrium potential and lateral interaction coefficient. Instead, this model only needs $f_H(E)$ and $f_{OH}(E)$, which are determined from experimental CVs.

With Pt(111) as the metal, I have $N_{ad} = 0.15$ Å^{-2} based on a lattice constant of 3.92 Å, and the potential of zero charge is $E_{pzc} = 0.29$ V_{SHE}.[101] Given that water dipole orientation lowers the pzc by 0.2 eV, E^0_{pzc} without considering this water dipole effect should be 0.49 V_{SHE}. In accordance with experiments by Ojha et al.,[21,22] I consider an electrolyte solution of 0.1 mM $HClO_4$ + x mM $LiClO_4$. The diameter of hydrated cations and anions is taken uniformly as $d_h = 7$ Å.

THE CASE WITHOUT CHEMISORBED IONS

The central formula expressed in eq 22 contains the interplay between the diffuse layer, water molecules at the ASP, and partially charged chemisorbed ions at the AIP. To simplify the matter, I consider in this section a simple case without chemisorbed ions, namely, $\theta_A = 0$ in eq 22. The focus is put on how chemical interactions between adsorbed water molecules and the metal influence the pzc and furthermore how field-dependent reorientation of water molecules changes the C_{dl} profile.

Influence of Metal−Water Interactions on the pzc

In the absence of chemisorbed ions, the pzc is obtained from eq 22 as

$$E_{pzc,SHE} = \chi_M - (\phi_{RE} - \phi_S)_{SHE} + \frac{N_{ad}}{\epsilon_2}\theta_w\mu_w\left(\coth(\delta\tilde{\mu}) - \frac{1}{\delta\tilde{\mu}}\right) \quad (25)$$

where the first term is the potential drop at the metal surface determined by the electron density profile at the interface, the second term is a constant of the SHE, and the third term represents the influence of water molecules at the ASP.

$E^0_{pzc,\ SHE}$ is defined as the value for the case of $\delta\tilde{\mu} = 0$, namely, the case in which metal−water interactions are the same for water molecules possessing $\alpha_w = 0°$ and $\alpha_w = 180°$. This artificial case is hardly met. In the general case of $\delta\tilde{\mu} \neq 0$, I obtain

$$E_{pzc,SHE} = E^0_{pzc,SHE} + \frac{N_{ad}}{\epsilon_2}\theta_w\mu_w\left(\coth(\delta\tilde{\mu}) - \frac{1}{\delta\tilde{\mu}}\right) \quad (26)$$

where the second term on the right-hand side represents the pzc shift due to orientational polarization of adsorbed water molecules. It is important to emphasize that the pzc shift due to electronic polarization of adsorbed water molecules is included in $E^0_{pzc,\ SHE}$.

When $|\delta\tilde{\mu}| \leq 1$, $E_{pzc,\ SHE}$ is asymptotic to

$$E_{pzc,SHE} = E^0_{pzc,SHE} + \frac{N_{ad}\theta_w\mu_w}{3\epsilon_2}\delta\tilde{\mu} \quad (27)$$

Equation 27 implies that $E_{pzc,\ SHE}$ is greater (smaller) than $E^0_{pzc,\ SHE}$ when $\delta\tilde{\mu} > 0$ (<0), as shown in Figure 3b. For the case of $\delta\tilde{\mu} < 0$, the first-layer water molecules prefer the $\alpha_w = 0°$ (H-up or O-down) configuration. For this case, the resulting potential rise due to the water dipole moment compensates partly for the potential drop at the metal surface, leading to a smaller $E_{pzc,\ SHE}$. In the opposite case, the first-layer water molecules prefer the $\alpha_w = 180°$ (H-down) configuration, resulting in an additional potential drop and thereby a higher $E_{pzc,\ SHE}$.

Influence of Water Orientational Polarization on C_{dl}

In this section, I analyze how water orientational polarization affects the differential double-layer capacitance C_{dl}. In addition to the full model, two simplified models are introduced to differentiate multiple coupled effects. The simplified model without ion size effects is described by a variant of eq 22 in the limit of $\gamma = 0$,

$$\frac{2RT}{F}\mathrm{arsinh}\left(\frac{F\lambda_D\sigma_{free}}{2RT\epsilon_b}\right) + \sigma_{free}\sum_{i=1,2,3}\frac{\delta_i}{\epsilon_i} - \frac{N_{ad}}{\epsilon_2}\theta_w\mu_w\langle\cos\alpha_w\rangle = E_{SHE} - E^0_{pzc,SHE} \quad (28)$$

In eq 28, I have neglected the chemisorption-induced dipole moment for this case without chemisorbed ions. The simplified model without water effects is expressed as a variant of eq 22 in the limit of $\theta_w = 0$,

$$\mathrm{sign}(\sigma_{free})\frac{2RT}{F}\mathrm{arsinh}\left(\sqrt{\frac{1}{2\gamma}\left(\exp\left(\frac{\gamma}{2}\left(\frac{F\lambda_D\sigma_{free}}{RT\epsilon_b}\right)^2\right) - 1\right)}\right) + \sigma_{free}\sum_{i=1,2,3}\frac{\delta_i}{\epsilon_i} = E_{SHE} - E^0_{pzc,SHE} \quad (29)$$

https://doi.org/10.1021/jacsau.2c00650
JACS Au XXXX, XXX, XXX−XXX

In Figure 4, I compare the three models for the case of $\delta\tilde{\mu} = 0$ with the base set of model parameters. The model without water

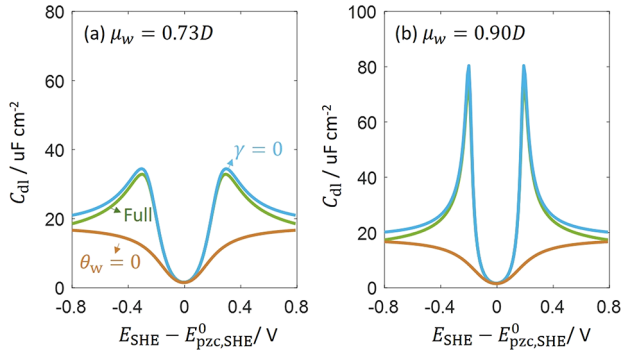

Figure 4. Differential double layer capacitance as a function of the electrode potential for the case of $\delta\tilde{\mu} = 0$ for two effective values of water dipole moment: (a) $\mu_w = 0.73$ D, (b) $\mu_w = 0.90$ D. $E^0_{pzc,\ SHE}$ represents the potential of zero charge without water dipole effects, which is used as the electrode potential reference here. Three models, including the full model, a simplified model without ion size effects, and a simplified model without water effects. The electrolyte solution is 0.1 mM $HClO_4$. $\delta\tilde{\mu} = 0$ and other model parameters have their base values. Matlab script of this figure is provided in the Supporting Information of this paper.

effects has a camel-shaped C_{dl} curve with two very broad peaks corresponding to overcrowding of counterions. The C_{dl} curve is symmetric around the pzc as I have neglected size asymmetry. Otherwise, the peak corresponding to smaller counterions will be higher, see, *e.g.*, ref 27.

Upon an increment in the magnitude of σ_{free}, adsorbed water molecules at the ASP could reduce the potential drop across the EDL via rearranging their orientations. Consequently, C_{dl} is increased due to water polarization effects, as seen in the comparison between the full model and the model without water effects. Equivalently, water molecules at the ASP contribute a negative capacitance in series with the diffuse layer capacitance, as pointed out earlier by Huang et al.[72] and Le et al.[53]

The two peaks of the C_{dl} curve become sharper and move closer to the pzc, compared to their counterparts of the model without water effects. The two peaks signify saturation of water polarization effect, rather than overcrowding of counterions in previous modified Poisson−Boltzmann theories.[28,29] Mathematically, it corresponds to $\langle \cos \alpha_w \rangle = 1$ or -1 depending on the sign of σ_{free}. These two peaks are significantly elevated when μ_w increases from the base value of 0.73 to 0.9 D, as shown in Figure 4b.

Since the electrolyte solution is ultradilute, $c_0 = 0.1$ mM, the ion size effect is unimportant near the pzc as the C_{dl} curves of the full model and the model without ion size effects overlap in the region of $|E_{SHE} - E^0_{pzc,\ SHE}| < 0.2$ V. As σ_{free} grows in magnitude and the EDL becomes more crowded with counterions, the ion size effect cannot be neglected any longer. Without considering the ion size effect, the two peaks are higher.

Figure 5a examines the influence of $\delta\tilde{\mu}$ on the C_{dl} curve. As already discussed, the pzc, corresponding to the valley of the C_{dl} curve, shifts to more negative electrode potentials as $\delta\tilde{\mu}$ goes negative. The C_{dl} curve becomes highly asymmetric with the left peak being much higher than the right one for $\delta\tilde{\mu} = -1$. A negative $\delta\tilde{\mu}$ means that in the absence of electrostatic interactions, water molecules prefer the configuration of $\alpha_w = 0°$ (the O-down or H-up configurations). Therefore, these water molecules have a higher capacity to screen negative σ_{free}, which

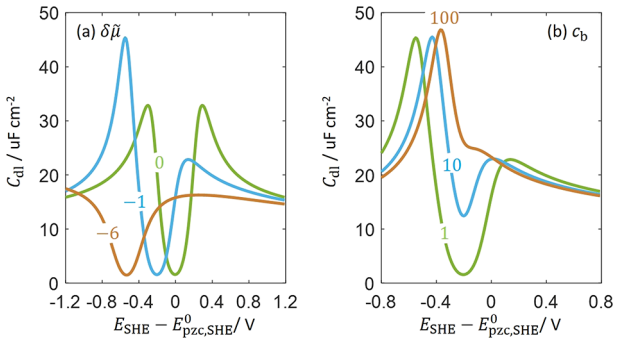

Figure 5. Differential double layer capacitance as a function of electrode potential for (a) different values of $\delta\tilde{\mu}$ normalized to thermal energy k_BT when the electrolyte concentration is 0.1 mM and (b) different electrolyte concentrations when $\delta\tilde{\mu} = -1$. $E^0_{pzc,\ SHE}$ represents the potential of zero charge without water dipole effects, which is used as the electrode potential reference here. Other model parameters have their base values. Matlab script of this figure is provided in the Supporting Information of this paper.

intends to rotate water molecules toward $\alpha_w = 180°$, than positive σ_{free}. Consequently, a higher C_{dl} peak is observed in the negatively charged region. Interestingly, the peak at the negatively charged surface almost disappears for $\delta\tilde{\mu} = -6$. For the case of such a very negative $\delta\tilde{\mu}$, the orientation of water molecules is dominated by the strong chemical interactions and is no longer tunable by the local electric field. Therefore, the C_{dl} curve resembles that of the model without water effects in Figure 4, except a horizontal shift due to $\delta\tilde{\mu}$.

Figure 5b examines the concentration dependence of the C_{dl} curve while $\delta\tilde{\mu} = -1$ is fixed. C_{dl} near the pzc is higher because the Debye length becomes smaller as the electrolyte concentration increases. In addition, the two peaks come closer in more concentrated electrolyte solution. These peaks are ascribed to saturation of water polarization. Let us denote as σ^c_{free} the critical magnitude of σ_{free} leading to saturated water polarization. At higher concentrations, C_{dl} is higher and σ^c_{free} can be achieved at a smaller potential difference away from the pzc.

THE CASE WITH CHEMISORBED IONS

Effect of Chemisorption-Induced Dipole Moment

Now chemisorption is brought into the play, and its influence on the C_{dl} curve is examined. Let us consider the Pt(111)−0.1 M $HClO_4$ interface. The CV of this interface is usually divided into a hydrogen adsorption region up to ~0.4 V_{RHE}, a hydroxyl adsorption region above ~0.55 V_{RHE}, and a double layer region in between. Climent et al. have conducted a comprehensive analysis of CVs of this interface at different temperatures using Frumkin isotherms.[91] Herein, a revisit from a different view assuming distributed equilibrium potentials of H_{ad} and OH_{ad} is presented, with the focus put on the effect of chemisorption-induced dipole moment on C_{dl}.

Figure 6a shows a model fitting of the CV within the potential range of [0.15, 0.75]V_{RHE} and a model-based decomposition of the total capacitance C_{tot} into C_{dl} and adsorption capacitances ($C_{H_{ad}}$ and $C_{OH_{ad}}$). The extracted distribution functions f_H and f_{OH}, defined in eq 6, are shown in Figure 6b. f_H is composed of four Gaussian functions with preset mean values of 0, 0.1, 0.2, and 0.3 V_{RHE}, and f_{OH} is composed of two Gaussian functions with preset mean values of 0.7 and 0.8 V_{RHE}. Twelve free

https://doi.org/10.1021/jacsau.2c00650
JACS Au XXXX, XXX, XXX−XXX

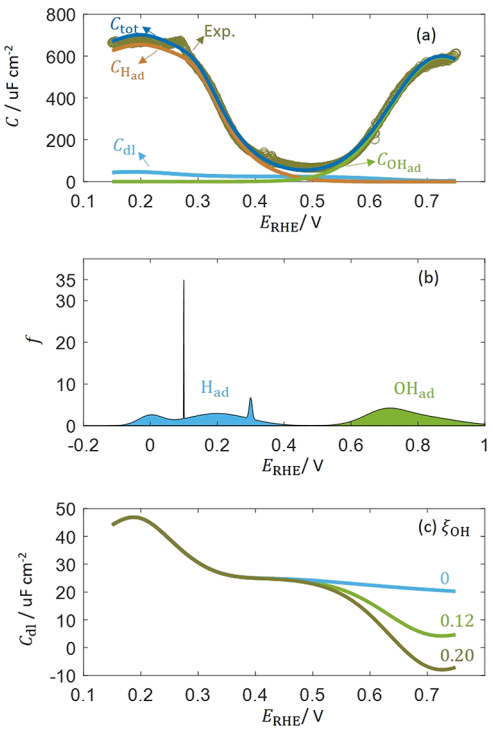

Figure 6. (a) Differential double-layer capacitance (C_{dl}), adsorption capacitance of H_{ad} and OH_{ad} ($C_{H_{ad}}$, $C_{OH_{ad}}$), and their sum (C_{tot}) for the double layer of Pt(111)−0.1 M $HClO_4$ interface. Experimental data, shown in circles, are taken from ref 22. (b) Model-based distributions of equilibrium potential of H and OH adsorption. (c) Comparison of differential double-layer capacitance for three values of the net electron number of OH_{ad}. The case of $\xi_{OH} = 0$ corresponds to the case without chemisorption-induced dipole moment, μ_{OH}. Matlab script of this figure is provided in the Supporting Information of this paper.

parameters are therefore the variances σ_k and weights p_k of these six distributions. Other EDL parameters have their base values. The basic idea of this approach resembles that of the distribution of relaxation times (DRT) proposed by von Schweidler in 1907; see a recent review on DRT.[102] The present approach could be termed distribution of chemisorption energies (DCE). A better fitting of C_{tot} can be obtained if a greater number of Gaussian functions are included, which is not the purpose of this work. The mere purpose of this fitting is to confirm that a Frumkin isotherm with repulsive lateral interactions can be mapped into a series of Langmuir isotherms with a DCE.

Figure 6a indicates that C_{dl} is a small percentage of C_{tot}. Figure 6c shows C_{dl} for the cases with and without $\Delta\phi_{ad}$ caused by chemisorption. Three values of the net electron number of OH_{ad}, ξ_{OH}, are compared, including the base value of 0.12, a zero value corresponding to the case of a complete charge transfer during chemisorption and hence a zero $\Delta\phi_{ad}$, and also a higher value of 0.20 to increase the magnitude of $\Delta\phi_{ad}$. When $\Delta\phi_{ad} = 0$, the C_{dl} curve contains a higher peak at ~0.2 V_{RHE}, and a much depressed peak at potentials more positive than $E_{pzc} = 0.29$ V_{SHE} (0.346 V_{RHE} for this case), similar to the results shown in Figure 5b. In comparison, C_{dl} drops above 0.5 V_{RHE} due to a positive $\Delta\phi_{ad}$ when $\xi_{OH} = 0.12$. Particularly, negative C_{dl} is found when $\xi_{OH} = 0.20$.

Negative C_{dl} means that σ_{free} decreases with increasing electrode potential, resulting in a nonmonotonic surface charging behavior. Chemisorption-induced nonmonotonic surface charging behaviors were revealed in a previous work[72] and elucidated in a, hopefully, more accessible manner recently.[80] The basic idea, as expressed in eq 1, is that negatively charged chemisorbed OH introduces a potential drop $\Delta\phi_{ad}$, which is tantamount to increasing the pzc. As a result, σ_{free} increases at a lower rate with the electrode potential, namely, a smaller C_{dl}, or decreases with the electrode potential, namely, a negative C_{dl}, depending on the magnitude of μ_{OH}.

Double Layer Region

Let us proceed to analyzing the recent experimental data by Ojha, Doblhoff-Dier, and Koper, focusing on the double layer region between 0.40 and 0.65 V_{RHE}.[22] In order to distance the pzc as much as possible from the hydrogen and hydroxyl adsorption/desorption regions, they delicately used 0.1 mM $HClO_4$ as the base electrolyte solution with a pH of 4, where the pzc is 0.53 V_{RHE}. They repeated the measurements on the Pt(111)−0.1 mM $HClO_4$ interface three times, allowing us to examine how experimental uncertainties affect model results in Figure 7. Afterward, experimental data in the presence of different concentrations of $LiClO_4$ are analyzed in Figure 8.

Figure 7a−c shows the model−experiment comparison for three pieces of capacitance data in 0.1 mM $HClO_4$. The EDL parameters are fixed at their base values, and the free fitting parameters are the weight p_k, expectations μ_k, and variances σ_k of distribution functions of H_{ad} and OH_{ad}. One Gaussian distribution for H_{ad} and two for OH_{ad} are sufficient in this narrow potential region. The fitted distributions are displayed in Figure 7d−f. The coverages of H_{ad} and OH_{ad} are shown in Figure 7g−i.

In Figure 7a−c, solid lines represent model results, and circles represent experimental data. The total capacitance (C_{total}) is further decomposed, with the aid of the model, into the capacitance due to H adsorption, $C_{H_{ad}}$, that is due to OH adsorption, $C_{OH_{ad}}$, and the pure double-layer capacitance, C_{dl}. The measured capacitance C_{total} is contributed majorly by pseudo-capacitances $C_{H_{ad}}$ and $C_{OH_{ad}}$. Three measurements show a moderate difference in between: the terrace in the potential range of 0.55−0.6 V_{RHE}, attributed to water adsorption in ref 22, almost disappears in the third measurement.

The present model attributes different profiles of C_{total} to variations in the distributed equilibrium potential of OH_{ad}, f_{OH}, as shown in Figure 7d−f. The OH adsorption has a bimodal normal distribution and the one at lower potentials with $p_1 < 6\%$ is responsible for the terrace of C_{total} in the potential range of 0.55−0.6 V_{RHE}. The terrace appears when the two normal distributions are well resolved, as in Figure 7d,e, and disappears when they come closer and become connected, as in Figure 7f. The variations in f_{OH} imply that the assumed distribution of equilibrium potential is likely affected by stochastic factors.

The coverages of adsorbed H_{ad} and OH_{ad}, denoted θ_H and θ_{OH}, are less than 5% in the double-layer region. However, such a small amount of adsorption results in adsorption capacitance several times higher than C_{dl}, which demonstrates the importance of and also difficulty in separating C_{dl} from adsorption capacitances for electrocatalytic double layers.

Experimental data in the presence of different concentrations of $LiClO_4$ are analyzed in Figure 8. The experiments were conducted on Pt(111) in 0.1 mM $HClO_4$ + x mM $LiClO_4$ (x = 0.1,0.3, 0.6, 1.0).[22] Experimental capacitance curves are shifted vertically in Figure 8a for visual clarity. The model results in solid lines neatly agree with experimental data in circles in the examined potential region. The fitted coverages of H_{ad} and

https://doi.org/10.1021/jacsau.2c00650
JACS Au XXXX, XXX, XXX−XXX

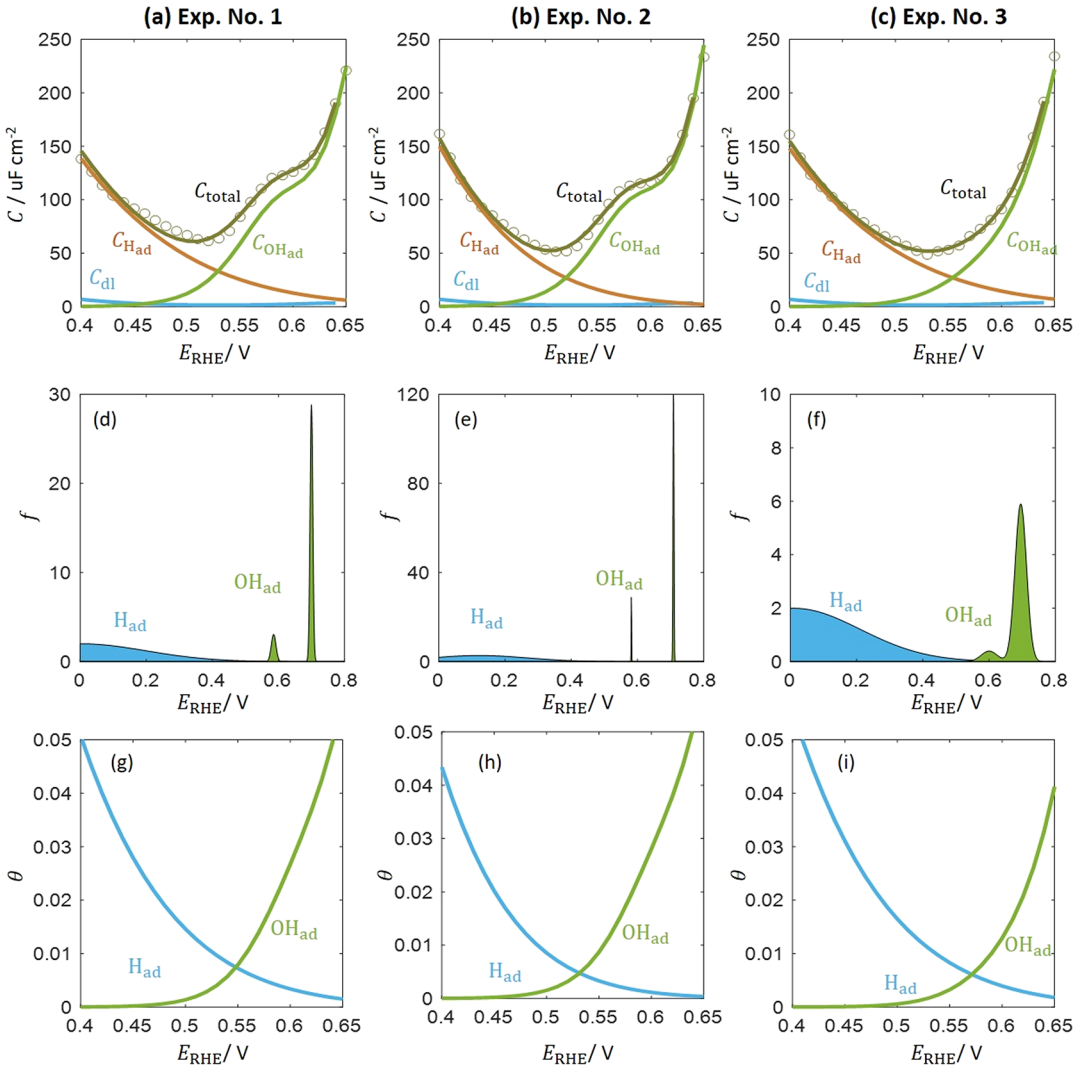

Figure 7. (a–c) Model–experiment comparison for the electric double layer at Pt(111)–aqueous interfaces. The experiment on a Pt(111) electrode in 0.1 mM $HClO_4$ was repeated three times.[22] Model results are marked as solid lines and experimental data as circles. The total capacitance (C_{total}) is decomposed into the capacitance due to H adsorption, $C_{H_{ad}}$, that is due to OH adsorption, $C_{OH_{ad}}$, and the pure double-layer capacitance, C_{dl}. (d–f) Model-based distributions of the equilibrium potential of H and OH adsorption. (g–i) Coverages of adsorbed H and OH. Matlab script of this figure is provided in the Supporting Information of this paper.

OH_{ad}, the pure double layer capacitance, and pseudo-capacitances of chemisorption are shown in Figure 8b–d, respectively. The correspondence between line colors and ionic concentrations indicated in Figure 8a is retained in all subfigures. As for the pure double-layer capacitance C_{dl} in Figure 8c, a Gouy–Chapman minimum is found at 0.53 V_{RHE}. The asymmetry around the pzc is caused by water adsorption. As shown in Figure 5a, a negative value of $\delta\tilde{\mu}$, namely, the O-down configuration is more favorable, results in a more tilted increase in C_{dl} when the electrode potential moves away from the pzc in the more negative direction. The valley and the terrace of the measured C_{total} shifts to lower potentials with increasing concentration of $LiClO_4$. In the present model, the shift in the capacitance minimum and terrace is associated with adsorption of OH, as shown in Figure 8d. Possible reasons for this are discussed in the next section.

DISCUSSION

Is There a Pure Double Layer Region at Pt(111)?

In contrast with previous works,[22,51,52] the present model maintains that voltammogram-derived capacitance of Pt(111) is majorly contributed by $C_{H_{ad}}$ and $C_{OH_{ad}}$ from a small percentage of active sites, Figure 8. One of the implications of this claim is that there is no pure double-layer region for the Pt(111) electrode.

The occurrence of chemisorbed OH_{ad} in the so-called double layer potential region could have two causes. On the one hand, there may be structural defects occupying a small percentage of the solid surface.[103,104] Adsorption of OH (H) occurs at lower (higher) potentials at these structural defects. In a study by Góez-Marín and Feliu,[105] they experimentally investigated the relation between oxygen reduction activity and step density and extrapolated this relation to obtain the oxygen reduction activity of an ideally defect-free Pt(111). They found that the extrapolated activity of this ideal Pt(111) is lower than that of a real Pt(111). This comparison leads them to conclude that "This is true even for those electrodes that do not apparently

https://doi.org/10.1021/jacsau.2c00650
JACS Au XXXX, XXX, XXX–XXX

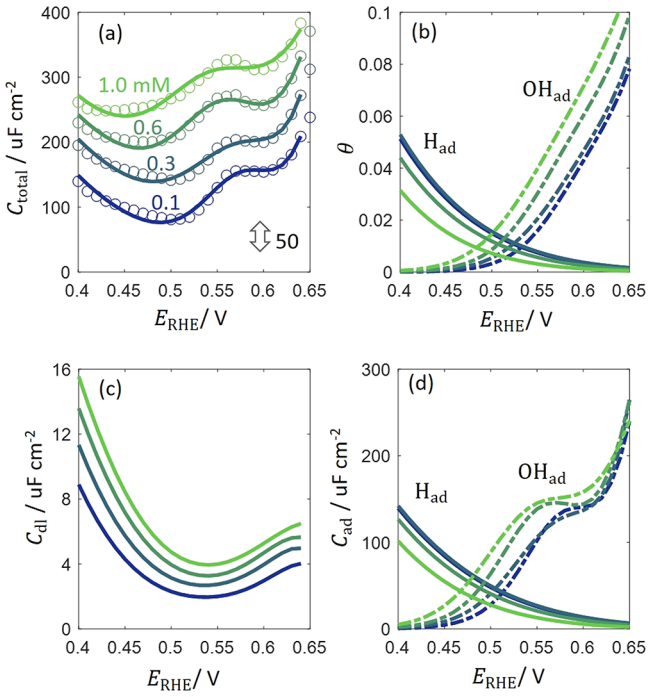

Figure 8. (a) Model−experiment comparison in the presence of different concentrations of $LiClO_4$ for the electric double layer at Pt(111) in 0.1 mM $HClO_4$ + *x* mM $LiClO_4$.[22] Model results are marked as solid lines and experimental data as circles. For the sake of clarity, a vertical shift of 50 between different lines is used in panel (a). Coverages of adsorbed (b) H_{ad} and OH_{ad}, (c) the pure double-layer capacitance, C_{dl}, and (d) adsorption capacitances $C_{H_{ad}}$ and $C_{OH_{ad}}$. Matlab script of this figure is provided in the Supporting Information of this paper.

show any step contribution signal in the blank voltammogram, pointing out that a real electrode has always surface defects." Recent works on stepped Pt electrodes, such as Pt(553)[106] and Pt(311),[107] have shown low-potential water dissociation in the hydrogen adsorption/desorption region, and the onset potential moves toward the "double layer" region at higher pHs.

On the other hand, interfacial water molecules have an energy distribution, as seen in AIMD simulations,[108] and higher-energy water molecules are decomposed and then adsorbed as OH_{ad} at lower potentials. Such a distribution, intrinsically stochastic to a certain extent, echoes the experimental uncertainties found in three repeated measurements on the Pt(111)−0.1 mM $HClO_4$ interface. Model results in Figure 8 further indicate that a higher concentration of $LiClO_4$ promotes earlier adsorption of OH. Berna et al. have adopted a similar idea to interpret chemisorption of OH at Pt(111).[109] Specifically, they attributed the broad peak in the low potential region and the sharp peak in the high potential region to the dissociation of two kinds of water molecules with different electrochemical potentials. Their treatment could be regarded as a special case of this model where the distribution function is actually composed of two delta functions.

Currently, it is hard to detect adsorbed intermediates at such a low coverage. Nevertheless, Kondo et al. deduced from their in situ surface X-ray scattering data that a small amount of oxygen-containing species (unspecified) and/or ClO_4^- is adsorbed on Pt(111) immersed in 0.1 M $HClO_4$ at 0.57 V_{RHE} within the double-layer region.[110] It has also been shown that the ClO_4^- concentration impacts the CV of Pt(111) in the double layer region.[110,111] Though I have assumed H_{ad} and OH_{ad} as the chemisorbates when explaining the experimental data of Ojha et al., the existence of other chemisorbates such as ClO_4^- and organic impurities cannot be excluded for this moment.[110,111]

Limitations and Possible Extensions of the Model

The present double layer model belongs to GCS-type models. An essential feature of these models is the decomposition of the double layer into several subregions, which are then described as dielectric continua. I am aware of the harsh criticisms on such GCS-type models regarding drastic simplifications of the double layer structure and its parameterization procedure that arbitrariness may slip in.[112] Nevertheless, it is undeniable that GCS-type models are simple yet effective in describing physicochemical properties of the double layer. Fortunately, accurate atomic details provided by careful first-principles calculations can help to avoid unphysical assumptions, omission of key factors, overparameterizaton and error cancellation, etc., in phenomenological modeling. Having said this, I stress that first-principles approaches have its own purpose, rather than just serving to elaborate phenomenological models.

Though the model results are obtained for a Pt(111) electrode in $HClO_4$-based solution, I do not see principal difficulties in applying it to the alkaline regime, to other electrolyte solution with specifically adsorbing anions such as sulfate and halide ions and to stepped Pt electrodes. In these new scenarios, the model needs to be extended by including new specific adsorption and/or chemisorption processes and to be re-parameterized on a case-by-case basis.

The model can be extended in the following directions in the future. First, the locations of chemisorbed ions and the first water layer, which are fixed in the present work, can be allowed to change as a function of electrode potential. Similar considerations of relaxation of the metal−solution gap have been shown to be able to bring forth negative C_{dl}.[113] Second, the model may also be extended to consider how electronic effects of chemisorbed ions and water molecules change χ_M.[65,114] Third, a constant $\delta\tilde{\mu}$ has been used so far, and it is meaningful to consider a potential-dependent change of $\delta\tilde{\mu}$, caused by interactions between chemisorbed ions and water molecules on the one hand and orientational dependency of water binding energy on the other.[115] Lastly, noncovalent interactions between chemisorbed ions and electrolyte species, key to understanding cation effects as shown in a recent study,[116] are also important factors to be treated. Lastly, the model can also be extended to study other chemisorption processes, including those of electrolyte anions and organic impurities, at different types of active sites.

CONCLUSIONS

A modified double layer model has been formulated for metal−aqueous interfaces in electrocatalytic systems. The present model divides the inner Helmholtz plane (IHP) further into an AIP (adsorbed ion plane) and ASP (adsorbed solvent plane), accounting for different locations of chemisorbed ions and solvent molecules. The present model employs a statistical treatment of the first-layer water molecules with chemical interactions imposed by the metal and a distributed treatment of chemisorption of electrolyte species.

The model shows that the potential of zero charge, pzc for short, depends on metal−water chemical interactions. I introduce $\delta\mu$ to characterize the chemical interaction energy difference between water dipoles of $\alpha_w = 0°$ and that of $\alpha_w = 180°$, where α_w is the angle between water dipole direction and the local electric field. It is found that the pzc becomes higher

https://doi.org/10.1021/jacsau.2c00650
JACS Au XXXX, XXX, XXX−XXX

(lower) when $\delta\mu > 0$ (<0). In addition to a shift in the pzc, the first-layer water molecules also dramatically elevate the double-layer capacitance C_{dl}. Equivalently, it means that the first-layer water molecules contribute a negative capacitance component in series with other components, which is a known effect. However, the formula derived in this work to describe this effect, eq 26, is, to my knowledge, a new contribution. The model also shows that chemisorption-induced dipole moment could lead to a new valley of the capacitance curve and the capacitance in the valley could take negative values.

The model is then employed to interpret recent CV-based capacitance data of Pt(111)−aqueous solution interfaces. The explanation is based on the ansatz that the experimental data are not the pure double-layer capacitance but include pseudo-capacitances of chemisorption of electrolyte species. This ansatz resolves the discrepancy that the CV-based capacitance values are several times higher than the values obtained using electrochemical impedance spectroscopy. In addition, it constitutes an alternative angle of understanding stochastic uncertainties found in these experiments. The ansatz and the resulting explanation, though being appealing, must be taken with care, as it implies that there is no pure double layer region even for Pt(111), an aspect that is yet to be confirmed.

Before closing, three experiments to confirm this ansatz are sketched here. One can examine the frequency dependence of interfacial capacitance in the double layer region, especially, at the pzc. If it is a pure double-layer capacitance, there should not be any frequency dispersion below the characteristic frequency of EDL capacitance, which is expressed as $f_{dl} \propto D/\lambda_D^2$ with D being the diffusion coefficient of electrolyte ions and λ_D being the Debye length, according to an exact analytical solution developed in ref 117. With typical values of $D = 10^{-9}$ m^{2}s^{-1} and $\lambda_D = 1 - 10$ nm, f_{dl} has a range of $10^7 - 10^9$ Hz. It is thus safe to claim that a pure double-layer capacitance should not depend on frequency below 1 MHz. In other words, shall one observe that the interfacial capacitance decreases with increasing frequency, it is very likely that the interfacial capacitance contains pseudo-capacitance(s). If it is difficult to obtain reliable high-frequency impedance data, a time-domain method that is easier to implement is to measure the current response to a potential step from the pzc by a small amount, say 20 mV. If it is pure double layer charging, the time constant, expressed as $t_{dl} \propto 10L\lambda_D/D$ with L being the thickness of the diffusion layer,[118] has a range of 1 − 10 ms using typical values of $D = 10^{-9}$ m^{2}s^{-1}, $L = 100\ \mu$m, and $\lambda_D = 1 - 10$ nm. In other words, shall one observe a current ramping with a time constant longer than 10 ms, it is very likely that other slower process(es) is (are) involved. The third experiment involves ultrafast CV measurements, which have been demonstrated on the order of megavolt per second,[119] and then check the scan-rate dependency of the obtained capacitance profiles. This would require careful ohmic drop compensation and noise control.

■ ASSOCIATED CONTENT

Data Availability Statement

No new experimental data. The scripts used to calculate the model results are available from the author upon request.

Supporting Information

The Supporting Information is available free of charge at https://pubs.acs.org/doi/10.1021/jacsau.2c00650.

Matlab scripts for reproducing results reported in this paper (PDF)

■ AUTHOR INFORMATION

Corresponding Author

Jun Huang − *Institute of Energy and Climate Research, IEK-13: Theory and Computation of Energy Materials, Forschungszentrum Jülich GmbH, 52425 Jülich, Germany;* orcid.org/0000-0002-1668-5361; Email: ju.huang@fz-juelich.de

Complete contact information is available at: https://pubs.acs.org/10.1021/jacsau.2c00650

Notes

The author declares no competing financial interest.

■ ACKNOWLEDGMENTS

This work is supported by the Alexander von Humboldt Foundation and the Helmholtz Young Investigators Group Leader Programme. I am grateful to Professors Gary Attard, Juan Feliu, Jianbo Zhang, Katharina Doblhoff-Dier, Ms. Lulu Zhang, and Mr. Jinwen Liu for helpful discussions.

■ REFERENCES

(1) Steinmann, S. N.; Seh, Z. W. Understanding electrified interfaces. *Nat. Rev. Mater.* **2021**, *6*, 289−291.

(2) Sebastián-Pascual, P.; Shao-Horn, Y.; Escudero-Escribano, M. Toward understanding the role of the electric double layer structure and electrolyte effects on well-defined interfaces for electrocatalysis. *Curr. Opin. Electrochem.* **2022**, *32*, 100918.

(3) Shin, S.-J.; Kim, D. H.; Bae, G.; Ringe, S.; Choi, H.; Lim, H.-K.; Choi, C. H.; Kim, H. On the importance of the electric double layer structure in aqueous electrocatalysis. *Nat. Commun.* **2022**, *13*, 174.

(4) Haid, R. W.; Ding, X.; Sarpey, T. K.; Bandarenka, A. S.; Garlyyev, B. Exploration of the electrical double-layer structure: Influence of electrolyte components on the double-layer capacitance and potential of maximum entropy. *Curr. Opin. Electrochem.* **2022**, *32*, 100882.

(5) Kozawa, A. Effects of anions and cations on oxygen reduction and oxygen evolution reactions on platinum electrodes. *J. Electroanal. Chem. (1959)* **1964**, *8*, 20−39.

(6) Strmcnik, D.; Kodama, K.; van der Vliet, D.; Greeley, J.; Stamenkovic, V. R.; Marković, N. M. The role of non-covalent interactions in electrocatalytic fuel-cell reactions on platinum. *Nat. Chem.* **2009**, *1*, 466−472.

(7) Strmcnik, D.; van der Vliet, D. F.; Chang, K. C.; Komanicky, V.; Kodama, K.; You, H.; Stamenkovic, V. R.; Marković, N. M. Effects of Li +, K+, and Ba2+ Cations on the ORR at Model and High Surface Area Pt and Au Surfaces in Alkaline Solutions. *J. Phys. Chem. Lett.* **2011**, *2*, 2733−2736.

(8) Suntivich, J.; Perry, E. E.; Gasteiger, H. A.; Shao-Horn, Y. The Influence of the Cation on the Oxygen Reduction and Evolution Activities of Oxide Surfaces in Alkaline Electrolyte. *Electrocatalysis* **2013**, *4*, 49−55.

(9) Resasco, J.; Chen, L. D.; Clark, E.; Tsai, C.; Hahn, C.; Jaramillo, T. F.; Chan, K.; Bell, A. T. Promoter Effects of Alkali Metal Cations on the Electrochemical Reduction of Carbon Dioxide. *J. Am. Chem. Soc.* **2017**, *139*, 11277−11287.

(10) Li, M. F.; Liao, L. W.; Yuan, D. F.; Mei, D.; Chen, Y.-X. pH effect on oxygen reduction reaction at Pt(111) electrode. *Electrochim. Acta* **2013**, *110*, 780−789.

(11) Briega-Martos, V.; Herrero, E.; Feliu, J. M. Effect of pH and Water Structure on the Oxygen Reduction Reaction on platinum electrodes. *Electrochim. Acta* **2017**, *241*, 497−509.

(12) Ledezma-Yanez, I.; Wallace, W. D. Z.; Sebastián-Pascual, P.; Climent, V.; Feliu, J. M.; Koper, M. T. M. Interfacial water reorganization as a pH-dependent descriptor of the hydrogen evolution rate on platinum electrodes. *Nat. Energy* **2017**, *2*, 17031.

(13) Rao, R. R.; Huang, B.; Katayama, Y.; Hwang, J.; Kawaguchi, T.; Lunger, J. R.; Peng, J.; Zhang, Y.; Morinaga, A.; Zhou, H.; You, H.; Shao-Horn, Y. pH- and Cation-Dependent Water Oxidation on Rutile RuO2(110). *J. Phys. Chem. C* **2021**, *125*, 8195−8207.
(14) Waegele, M. M.; Gunathunge, C. M.; Li, J.; Li, X. How cations affect the electric double layer and the rates and selectivity of electrocatalytic processes. *J. Chem. Phys.* **2019**, *151*, 160902.
(15) Colic, V.; Pohl, M. D.; Scieszka, D.; Bandarenka, A. S. Influence of the electrolyte composition on the activity and selectivity of electrocatalytic centers. *Catal. Today* **2016**, *262*, 24−35.
(16) Moura de Salles Pupo, M.; Kortlever, R. Electrolyte Effects on the Electrochemical Reduction of CO2. *ChemPhysChem* **2019**, *20*, 2926−2935.
(17) Deng, B.; Huang, M.; Zhao, X.; Mou, S.; Dong, F. Interfacial Electrolyte Effects on Electrocatalytic CO2 Reduction. *ACS Catal.* **2022**, *12*, 331−362.
(18) Pajkossy, T.; Kolb, D. M. Double layer capacitance of Pt(111) single crystal electrodes. *Electrochim. Acta* **2001**, *46*, 3063−3071.
(19) Pajkossy, T. Voltammetry and Impedance of Pt(111) Electrodes in Aqueous KClO4 Solutions. *Zeitschrift für Physikalische Chemie* **2003**, *217*, 351.
(20) Pajkossy, T.; Kolb, D. M. On the origin of the double layer capacitance maximum of Pt(111) single crystal electrodes. *Electrochem. Commun.* **2003**, *5*, 283−285.
(21) Ojha, K.; Arulmozhi, N.; Aranzales, D.; Koper, M. T. M. Double Layer at the Pt(111)−Aqueous Electrolyte Interface: Potential of Zero Charge and Anomalous Gouy−Chapman Screening. *Angew. Chem.* **2020**, *59*, 711−715.
(22) Ojha, K.; Doblhoff-Dier, K.; Koper Marc, T. M. Double-layer structure of the Pt(111)−aqueous electrolyte interface. *Proc. Natl. Acad. Sci.* **2022**, *119*, No. e2116016119.
(23) Xue, S.; Garlyyev, B.; Auer, A.; Kunze-Liebhäuser, J.; Bandarenka, A. S. How the Nature of the Alkali Metal Cations Influences the Double-Layer Capacitance of Cu, Au, and Pt Single-Crystal Electrodes. *J. Phys. Chem. C* **2020**, *124*, 12442−12447.
(24) Schmickler, W.; Santos, E., *Interfacial electrochemistry*. Springer-Verlag Berlin Heidelberg: New York, 2010; p XII, 270.
(25) Guidelli, R.; Schmickler, W. Recent developments in models for the interface between a metal and an aqueous solution. *Electrochim. Acta* **2000**, *45*, 2317−2338.
(26) Damaskin, B. B.; Petrii, O. A. Historical development of theories of the electrochemical double layer. *J. Solid State Electrochem.* **2011**, *15*, 1317−1334.
(27) Zhang, L. L.; Li, C. K.; Huang, J. A Beginners' Guide to Modelling of Electric Double Layer Under Equilibrium, Non-equilibrium and AC Conditions. *J. Electrochem.* **2022**, *28*, 2108471.
(28) Kornyshev, A. A. Double-Layer in Ionic Liquids: Paradigm Change? *J. Phys. Chem. B* **2007**, *111*, 5545−5557.
(29) Budkov, Y. A.; Kolesnikov, A. L. Electric double layer theory for room temperature ionic liquids on charged electrodes: Milestones and prospects. *Curr. Opin. Electrochem.* **2022**, *33*, 100931.
(30) Gouy, G. Sur La Constitution De La Charge Electrique A La Surface D'Un Electrolyte. *J. Phys. Theor. Appl.* **1910**, *9*, 457−468.
(31) Grahame, D. C. The Electrical Double Layer and the Theory of Electrocapillarity. *Chem. Rev.* **1947**, *41*, 441−501.
(32) Parsons, R. The electrical double layer: recent experimental and theoretical developments. *Chem. Rev.* **1990**, *90*, 813−826.
(33) Mott, N. F.; Watts-Tobin, R. J. The interface between a metal and an electrolyte. *Electrochim. Acta* **1961**, *4*, 79−107.
(34) Watts-tobin, R. J. The interface between a metal and an electrolytic solution. *Philos. Mag.* **1961**, *6*, 133−153.
(35) Macdonald, J. R.; Barlow, C. A. Theory of Double-Layer Differential Capacitance in Electrolytes. *J. Chem. Phys.* **1962**, *36*, 3062−3080.
(36) Bockris, J. O. M.; Habib, M. A. Contributions of water dipoles to double layer properties: A three-state water model. *Electrochim. Acta* **1977**, *22*, 41−46.
(37) Levine, S.; Bell, G. M.; Calvert, D. THE DISCRETENESS-OF-CHARGE EFFECT IN ELECTRIC DOUBLE LAYER THEORY. *Can. J. Chem.* **1962**, *40*, 518−538.
(38) Fawcett, W. R.; Levine, S. Discreteness-of-charge effects in electrode kinetics. *J. Electroanal. Chem. Interfacial Electrochem.* **1973**, *43*, 175−184.
(39) Grahame, D. C. Discreteness-of-charge-effects in the inner region of the electrical double layer. *Zeitschrift für Elektrochemie, Berichte der Bunsengesellschaft für physikalische Chemie* **1958**, *62*, 264−274.
(40) Fawcett, W. R. Fifty years of studies of double layer effects in electrode kinetics—a personal view. *J. Solid State Electrochem.* **2011**, *15*, 1347.
(41) Badiali, J. P.; Rosinberg, M. L.; Goodisman, J. Contribution of the metal to the differential capacity of an ideally polarisable electrode. *J. Electroanal. Chem.* **1983**, *143*, 73−88.
(42) Badiali, J. P.; Rosinberg, M. L.; Vericat, F.; Blum, L. A microscopic model for the liquid metal-ionic solution interface. *J. Electroanal. Chem.* **1983**, *158*, 253−267.
(43) Schmickler, W. A jellium-dipole model for the double layer. *J. Electroanal. Chem.* **1983**, *150*, 19−24.
(44) Kornyshev, A. A. Metal electrons in the double layer theory. *Electrochim. Acta* **1989**, *34*, 1829−1847.
(45) Valette, G. Double layer on silver single-crystal electrodes in contact with electrolytes having anions which present a slight specific adsorption: Part I. The (110) face. *J. Electroanal. Chem. Interfacial Electrochem.* **1981**, *122*, 285−297.
(46) Valette, G. Double layer on silver single crystal electrodes in contact with electrolytes having anions which are slightly specifically adsorbed: Part II. The (100) face. *J. Electroanal. Chem. Interfacial Electrochem.* **1982**, *138*, 37−54.
(47) Valette, G. Double layer on silver single crystal electrodes in contact with electrolytes having anions which are slightly specifically adsorbed: Part III. The (111) face. *J. Electroanal. Chem. Interfacial Electrochem.* **1989**, *269*, 191−203.
(48) Hamelin, A.; Foresti, M. L.; Guidelli, R. Test of the Gouy-Chapman theory at a (111) silver single-crystal electrode. *J. Electroanal. Chem.* **1993**, *346*, 251−259.
(49) Pajkossy, T.; Kolb, D. M. Double layer capacitance of the platinum group metals in the double layer region. *Electrochem. Commun.* **2007**, *9*, 1171−1174.
(50) Schouten, K. J. P.; van der Niet, M. J. T. C.; Koper, M. T. M. Impedance spectroscopy of H and OH adsorption on stepped single-crystal platinum electrodes in alkaline and acidic media. *Phys. Chem. Chem. Phys.* **2010**, *12*, 15217−15224.
(51) Doblhoff-Dier, K.; Koper, M. T. M. Modeling the Gouy−Chapman Diffuse Capacitance with Attractive Ion−Surface Interaction. *J. Phys. Chem. C* **2021**, *125*, 16664−16673.
(52) Schmickler, W. The Effect of Weak Adsorption on the Double Layer Capacitance. *ChemElectroChem* **2021**, *8*, 4218−4222.
(53) Le, J.-B.; Fan, Q.-Y.; Li, J.-Q.; Cheng, J. Molecular origin of negative component of Helmholtz capacitance at electrified Pt(111)/water interface. *Sci. Adv.* **2021**, *6*, No. eabb1219.
(54) Sibert, E.; Faure, R.; Durand, R. High frequency impedance measurements on Pt(111) in sulphuric and perchloric acids. *J. Electroanal. Chem.* **2001**, *515*, 71−81.
(55) Grahame, D. C. Components of Charge and Potential in the Non-diffuse Region of the Electrical Double Layer: Potassium Iodide Solutions in Contact with Mercury at 25°1. *J. Am. Chem. Soc.* **1958**, *80*, 4201−4210.
(56) Grahame, D. C.; Parsons, R. Components of Charge and Potential in the Inner Region of the Electrical Double Layer: Aqueous Potassium Chloride Solutions in Contact with Mercury at 25°. *J. Am. Chem. Soc.* **1961**, *83*, 1291−1296.
(57) Damaskin, B.; Pankratova, I.; Palm, U.; Anni, K.; Väärtnõu, M.; Salve, M. Comparison of the ionic adsorption theories for the electrode/solution interface by computer simulation. *J. Electroanal. Chem. Interfacial Electrochem.* **1987**, *234*, 31−53.
(58) Kolotyrkin, Y. M.; Alexeyev, Y. V.; Popov, Y. A. Double layer model taking into account the specific adsorption of ions: Application

https://doi.org/10.1021/jacsau.2c00650
JACS Au XXXX, XXX, XXX−XXX

to the process of hydrogen adsorption on lead in the presence of iodide ion. *J. Electroanal. Chem. Interfacial Electrochem.* **1975**, *62*, 135−149.
(59) Vorotyntsev, M. Chemisorption theory for charged species at electrodes in the model of an energetically homogeneous surface. *J. Res. Inst. Catal., Hokkaido Univ.* **1983**, *30*, 167−177.
(60) Guidelli, R., Monolayer Models of Metal-Water Interphases and their use in the Interpretation of Differential Capacity Curves and of Organic Adsorption. In *Trends in Interfacial Electrochemistry*, Silva, A. F., Ed. Springer Netherlands: Dordrecht, 1986; pp. 387−452, DOI: 10.1007/978-94-009-4694-1_15.
(61) Trasatti, S. Work function, electronegativity, and electrochemical behaviour of metals: II. Potentials of zero charge and "electrochemical" work functions. *J. Electroanal. Chem. Interfacial Electrochem.* **1971**, *33*, 351−378.
(62) Damaskin, B. B.; Frumkin, A. N. Potentials of zero charge, interaction of metals with water and adsorption of organic substances—III. The role of the water dipoles in the structure of the dense part of the electric double layer. *Electrochim. Acta* **1974**, *19*, 173−176.
(63) Bockris, J. O. M.; Devanathan, M. A. V.; Müller, K. On the structure of charged interfaces. *Proc. Roy. Soc. A* **1963**, *274*, 55−79.
(64) Sakong, S.; Forster-Tonigold, K.; Groß, A. The structure of water at a Pt(111) electrode and the potential of zero charge studied from first principles. *J. Chem. Phys.* **2016**, *144*, 194701.
(65) Le, J.; Iannuzzi, M.; Cuesta, A.; Cheng, J. Determining Potentials of Zero Charge of Metal Electrodes versus the Standard Hydrogen Electrode from Density-Functional-Theory-Based Molecular Dynamics. *Phys. Rev. Lett.* **2017**, *119*, No. 016801.
(66) Sakong, S.; Groß, A. The electric double layer at metal-water interfaces revisited based on a charge polarization scheme. *J. Chem. Phys.* **2018**, *149*, No. 084705.
(67) Le, J.-B.; Chen, A.; Li, L.; Xiong, J.-F.; Lan, J.; Liu, Y.-P.; Iannuzzi, M.; Cheng, J. Modeling Electrified Pt(111)-Had/Water Interfaces from Ab Initio Molecular Dynamics. *JACS Au* **2021**, *1*, 569−577.
(68) Groß, A.; Sakong, S. Ab Initio Simulations of Water/Metal Interfaces. *Chem. Rev.* **2022**, 10746.
(69) Schmickler, W.; Guidelli, R. The partial charge transfer. *Electrochim. Acta* **2014**, *127*, 489−505.
(70) Carnie, S. L.; Chan, D. Y. C. The modelling of solvent structure in the electrical double layer. *Adv. Colloid Interface Sci.* **1982**, *16*, 81−100.
(71) Schmickler, W.; Guidelli, R. Ionic adsorption and the surface dipole potential. *J. Electroanal. Chem. Interfacial Electrochem.* **1987**, *235*, 387−392.
(72) Huang, J.; Malek, A.; Zhang, J.; Eikerling, M. H. Non-monotonic Surface Charging Behavior of Platinum: A Paradigm Change. *J. Phys. Chem. C* **2016**, *120*, 13587−13595.
(73) Huang, J.; Zhou, T.; Zhang, J.; Eikerling, M. Double layer of platinum electrodes: Non-monotonic surface charging phenomena and negative double layer capacitance. *J. Chem. Phys.* **2018**, *148*, No. 044704.
(74) Zhang, M.-K.; Cai, J.; Chen, Y.-X. On the electrode charge at the metal/solution interface with specific adsorption. *Curr. Opin. Electrochem.* **2022**, *36*, 101161.
(75) Frumkin, A. N.; Petrii, O. A. Potentials of zero total and zero free charge of platinum group metals. *Electrochim. Acta* **1975**, *20*, 347−359.
(76) Damaskin, B. B.; Safonov, V. A.; Petrii, O. A. Model of two limiting states for describing the properties of the electric double layer in the absence of specific adsorption of ions. *J. Electroanal. Chem. Interfacial Electrochem.* **1989**, *258*, 13−25.
(77) Safonov, V. A.; Krivenko, A. G.; Choba, M. A. Initial oxidation of silver electrode in weakly acidic sodium fluoride solutions: Potential shifts induced by laser heating. *Electrochim. Acta* **2008**, *53*, 4859−4866.
(78) Garcia-Araez, N.; Climent, V.; Feliu, J. Potential-Dependent Water Orientation on Pt(111), Pt(100), and Pt(110), As Inferred from Laser-Pulsed Experiments. Electrostatic and Chemical Effects. *J. Phys. Chem. C* **2009**, *113*, 9290−9304.
(79) Sarabia, F. J.; Sebastián, P.; Climent, V.; Feliu, J. M. New insights into the Pt(hkl)-alkaline solution interphases from the laser induced temperature jump method. *J. Electroanal. Chem.* **2020**, *872*, 114068.
(80) Huang, J. Surface charging behaviors of electrocatalytic interfaces with partially charged chemisorbates. *Curr. Opin. Electrochem.* **2022**, *33*, 100938.
(81) Gongadze, E.; Iglič, A. Decrease of permittivity of an electrolyte solution near a charged surface due to saturation and excluded volume effects. *Bioelectrochemistry* **2012**, *87*, 199−203.
(82) Levy, A.; Andelman, D.; Orland, H. Dipolar Poisson-Boltzmann approach to ionic solutions: A mean field and loop expansion analysis. *J. Chem. Phys.* **2013**, *139*, 164909.
(83) Braunwarth, L.; Jung, C.; Jacob, T. Potential-Dependent Pt(111)/Water Interface: Tackling the Challenge of a Consistent Treatment of Electrochemical Interfaces**. *ChemPhysChem* **2022**, *n/a*, No. e202200336.
(84) Kastlunger, G.; Lindgren, P.; Peterson, A. A. Controlled-Potential Simulation of Elementary Electrochemical Reactions: Proton Discharge on Metal Surfaces. *J. Phys. Chem. C* **2018**, *122*, 12771−12781.
(85) Foresti, M. L.; Innocenti, M.; Forni, F.; Guidelli, R. Electrosorption Valency and Partial Charge Transfer in Halide and Sulfide Adsorption on Ag(111). *Langmuir* **1998**, *14*, 7008−7016.
(86) Zhang, Y.; Huang, J. Treatment of Ion-Size Asymmetry in Lattice-Gas Models for Electrical Double Layer. *J. Phys. Chem. C* **2018**, *122*, 28652−28664.
(87) Qing, L.; Jiang, J. Double-Edged Sword of Ion-Size Asymmetry in Energy Storage of Supercapacitors. *J. Phys. Chem. Lett.* **2022**, *13*, 1438−1445.
(88) Bossa, G. V.; Caetano, D. L. Z.; de Carvalho, S. J.; May, S. Differential capacitance of an electrical double layer with asymmetric ion sizes in the presence of hydration interactions. *Electrochim. Acta* **2019**, *321*, 134655.
(89) Gongadze, E.; Iglič, A. Asymmetric size of ions and orientational ordering of water dipoles in electric double layer model - an analytical mean-field approach. *Electrochim. Acta* **2015**, *178*, 541−545.
(90) Garcia-Araez, N.; Climent, V.; Feliu, J. M. Analysis of temperature effects on hydrogen and OH adsorption on Pt(111), Pt(100) and Pt(110) by means of Gibbs thermodynamics. *J. Electroanal. Chem.* **2010**, *649*, 69−82.
(91) Climent, V.; Góez, R.; Orts, J. M.; Feliu, J. M. Thermodynamic Analysis of the Temperature Dependence of OH Adsorption on Pt(111) and Pt(100) Electrodes in Acidic Media in the Absence of Specific Anion Adsorption. *J. Phys. Chem. B* **2006**, *110*, 11344−11351.
(92) Hörmann, N. G.; Reuter, K. Thermodynamic cyclic voltammograms: peak positions and shapes. *J. Phys.: Condens. Matter* **2021**, *33*, 264004.
(93) Huang, J. Hybrid density-potential functional theory of electric double layers. *Electrochim. Acta* **2021**, *389*, 138720.
(94) Trasatti, S. The "absolute" electrode potential—the end of the story. *Electrochim. Acta* **1990**, *35*, 269−271.
(95) Melander, M.; Wu, T.; Honkala, K. Constant inner potential DFT for modelling electrochemical systems under constant potential and bias. *ChemRxiv* **2022**, DOI: 10.26434/chemrxiv-2021-r621x-v2, This content is a preprint and has not been peer-reviewed..
(96) Putintsev, N. M.; Putintsev, D. N. High-frequency dielectric permittivity of water and its components. *Russ. J. Phys. Chem. A* **2011**, *85*, 1113−1118.
(97) Schnur, S.; Groß, A. Properties of metal−water interfaces studied from first principles. *New J. Phys.* **2009**, *11*, 125003.
(98) Sakong, S.; Groß, A. Water structures on a Pt(111) electrode from ab initio molecular dynamic simulations for a variety of electrochemical conditions. *Phys. Chem. Chem. Phys.* **2020**, *22*, 10431−10437.
(99) Abrashkin, A.; Andelman, D.; Orland, H. Dipolar Poisson-Boltzmann Equation: Ions and Dipoles Close to Charge Interfaces. *Phys. Rev. Lett.* **2007**, *99*, No. 077801.
(100) Malek, A.; Eikerling, M. H. Chemisorbed Oxygen at Pt(111): a DFT Study of Structural and Electronic Surface Properties. *Electrocatalysis* **2018**, *9*, 370−379.

(101) Martínez-Hincapié, R.; Sebastián-Pascual, P.; Climent, V.; Feliu, J. M. Exploring the interfacial neutral pH region of Pt(111) electrodes. *Electrochem. Commun.* **2015**, *58*, 62−64.
(102) Kobayashi, K.; Suzuki, T. S. Distribution of Relaxation Time Analysis for Non-ideal Immittance Spectrum: Discussion and Progress. *J. Phys. Soc. Jpn.* **2018**, *87*, No. 094002.
(103) Fernández, P. S.; Tereshchuk, P.; Angelucci, C. A.; Gomes, J. F.; Garcia, A. C.; Martins, C. A.; Camara, G. A.; Martins, M. E.; Da Silva, J. L. F.; Tremiliosi-Filho, G. How do random superficial defects influence the electro-oxidation of glycerol on Pt(111) surfaces? *Phys. Chem. Chem. Phys.* **2016**, *18*, 25582−25591.
(104) Nie, S.; Feibelman, P. J.; Bartelt, N. C.; Thürmer, K. Pentagons and Heptagons in the First Water Layer on Pt(111). *Phys. Rev. Lett.* **2010**, *105*, No. 026102.
(105) Góez-Marín, A. M.; Feliu, J. M. Oxygen reduction on nanostructured platinum surfaces in acidic media: Promoting effect of surface steps and ideal response of Pt(111). *Catal. Today* **2015**, *244*, 172−176.
(106) Chen, X.; McCrum, I. T.; Schwarz, K. A.; Janik, M. J.; Koper, M. T. M. Co-adsorption of Cations as the Cause of the Apparent pH Dependence of Hydrogen Adsorption on a Stepped Platinum Single-Crystal Electrode. *Angew. Chem.* **2017**, *56*, 15025−15029.
(107) Rizo, R.; Fernández-Vidal, J.; Hardwick, L. J.; Attard, G. A.; Vidal-Iglesias, F. J.; Climent, V.; Herrero, E.; Feliu, J. M. Investigating the presence of adsorbed species on Pt steps at low potentials. *Nat. Commun.* **2022**, *13*, 2550.
(108) Korpelin, V.; Kiljunen, T.; Melander, M. M.; Caro, M. A.; Kristoffersen, H. H.; Mammen, N.; Apaja, V.; Honkala, K. Addressing Dynamics at Catalytic Heterogeneous Interfaces with DFT-MD: Anomalous Temperature Distributions from Commonly Used Thermostats. *J. Phys. Chem. Lett.* **2022**, *13*, 2644−2652.
(109) Berná, A.; Climent, V.; Feliu, J. M. New understanding of the nature of OH adsorption on Pt(111) electrodes. *Electrochem. Commun.* **2007**, *9*, 2789−2794.
(110) Kondo, T.; Masuda, T.; Aoki, N.; Uosaki, K. Potential-Dependent Structures and Potential-Induced Structure Changes at Pt(111) Single-Crystal Electrode/Sulfuric and Perchloric Acid Interfaces in the Potential Region between Hydrogen Underpotential Deposition and Surface Oxide Formation by In Situ Surface X-ray Scattering. *J. Phys. Chem. C* **2016**, *120*, 16118−16131.
(111) Attard, G. A.; Brew, A.; Hunter, K.; Sharman, J.; Wright, E. Specific adsorption of perchlorate anions on Pt{hkl} single crystal electrodes. *Phys. Chem. Chem. Phys.* **2014**, *16*, 13689−13698.
(112) Schmickler, W. Double layer theory. *J. Solid State Electrochem.* **2020**, *24*, 2175−2176.
(113) Partenskii, M. B.; Jordan, P. C. Relaxing gap capacitor models of electrified interfaces. *Am. J. Phys.* **2010**, *79*, 103−110.
(114) Zhu, J.-X.; Le, J.-B.; Koper, M. T. M.; Doblhoff-Dier, K.; Cheng, J. Effects of Adsorbed OH on Pt(100)/Water Interfacial Structures and Potential. *J. Phys. Chem. C* **2021**, *125*, 21571−21579.
(115) Clabaut, P.; Staub, R.; Galiana, J.; Antonetti, E.; Steinmann, S. N. Water adlayers on noble metal surfaces: Insights from energy decomposition analysis. *J. Chem. Phys.* **2020**, *153*, No. 054703.
(116) Ovalle, V. J.; Hsu, Y.-S.; Agrawal, N.; Janik, M. J.; Waegele, M. M. Correlating hydration free energy and specific adsorption of alkali metal cations during CO2 electroreduction on Au. *Nat. Catal.* **2022**, *5*, 624−632.
(117) Li, C. K.; Huang, J. Impedance Response of Electrochemical Interfaces: Part I. Exact Analytical Expressions for Ideally Polarizable Electrodes. *J. Electrochem. Soc.* **2021**, *167*, 166517.
(118) Huang, J. On obtaining double-layer capacitance and potential of zero charge from voltammetry. *J. Electroanal. Chem.* **2020**, *870*, 114243.
(119) Amatore, C.; Maisonhaute, E.; Simonneau, G. Ohmic drop compensation in cyclic voltammetry at scan rates in the megavolt per second range: access to nanometric diffusion layers via transient electrochemistry. *J. Electroanal. Chem.* **2000**, *486*, 141−155.

https://doi.org/10.1021/jacsau.2c00650
JACS Au XXXX, XXX, XXX−XXX